Norwegian Meteorological Institute
met.no

met.no report

Report no. 5/2007
Oceanography
ISSN: 1503-8025
Oslo, May 18, 2007

CONMAN Technical Report No. 2: Analysis of model results

J. H. LaCasce, L. P. Røed, L. Bertino and B. Ådlandsvik

with contributions from
J. Albretsen, W. P. Budgell, H. Engedahl, C. Hansen, J. A. Johannessen and E. Svendsen[1]:

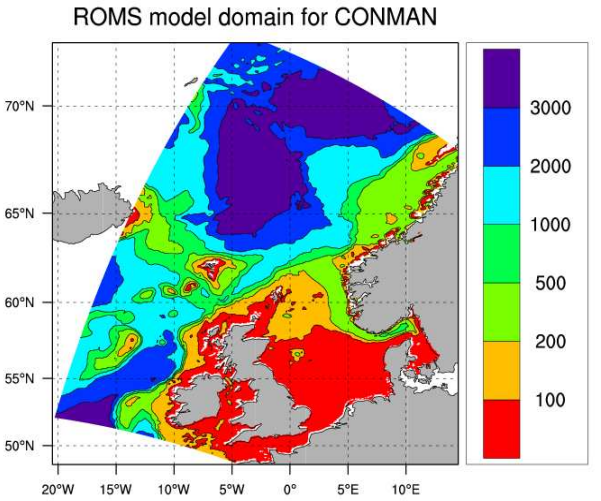

[1]Jon Albretsen, Harald Engedahl, Joseph H. LaCasce and Lars Petter Røed are affiliated with the Norwegian Meteorological Institute (met.no), Oslo, Norway,
W. Paul Budgell, Einar Svendsen and Bjørn Ådlandsvik are affiliated with Insitute of Marine Research (IMR), Bergen, Norway
Laurent Bertino, Johnny A. Johannessen and Cecilie Hansen are affiliated with the Nansen Environmental and Remote Sensing Center/Mohn-Sverdrup Center (NERSC/MSC), Bergen, Norway
Joseph H. LaCasce and Lars Petter Røed are also affiliated with the Department of Geosciences, Section Meteorology and Oceanography, University of Oslo, Norway

Norwegian Meteorological Institute
met.no

report

Number	Subject	Date	Classification	ISSN
5/2007	Oceanography	May 18, 2007	☒ Open ☐ Restricted ☐ Confidential	1503-8025

Title

CONMAN Technical Report No. 2: Analysis of model results

Authors

J. H. LaCasce, L. P. Røed, L. Bertino and B. Ådlandsvik

Client(s)	Client reference
Norwegian Deepwater Programme, MetOcean Project	Hans J. Sætre, AS Norske Shell

Abstract

We compare the results from a three year simulation with the three eddy-permitting numerical ocean models MIPOM, ROMS and HYCOM, for a limited area of the northeastern Atlantic Ocean. The forcing, boundary conditions and model set ups were chosen to be as similar as possible. We validate the model velocities by comparing them to those derived from in situ data, from current meters and from satellite altimetry. No validation against water masses is performed. Since the available observations generally do not overlap in time with the model simulations and that there may be significant year to year variability, we focus on statistical comparisons using time series longer than two years. We find that the MIPOM and HYCOM velocities are consistently too weak, and that their means deviate from the observed means in both path and direction, and MIPOM more so than HYCOM. The ROMS velocities are more energetic and compare more favorably with in situ observations, as do the ROMS-derived means. We believe that the success of ROMS is due its more sophisticated numerics. As a result ROMS is better at capturing the high velocity events of importance for, e.g., design purposes. Based on the analysis we therefore recommend to use ROMS in future numerical ocean prediction systems for Norwegian waters.

Keywords

Physical Oceanography, Numerical Modeling, Mesoscale

Disiplinary signature	Responsible signature
Eivind A. Martinsen, Head Section Oceanography	Øystein Hov, Head Research and Development Department

Postal address PO Box 43 Blindern, N-0313 Oslo, Norway
Office Niels Henrik Abels vei 40
Telephone +47 2296 3000
Telefax +47 2296 3050
e-mail: met.inst@met.no **Web:** met.no
Bank account 7695 05 00601
Swift code DNBANOKK

Executive summary

We consider the results from a three year simulation employing three eddy-permitting numerical ocean models. Two of them are local versions of the terrain-following coordinate models POM (Princeton Ocean Model, *Blumberg and Mellor*, 1987) and ROMS (Regional Ocean Modeling System, *Shchepetkin and McWilliams*, 2005). The third is a local version of the hybrid coordinate model HYCOM (HYbrid Coordinate Ocean Model, *Bleck*, 2002; *Chassignet et al.*, 2003).

The local version of POM we use is MIPOM (*Engedahl*, 1995b; *Engedahl et al.*, 2001; *Røed and Fossum*, 2004; *LaCasce and Engedahl*, 2005). It is currently the main ocean prediction model at the Norwegian Meteorological Institute (**met.no**). MIPOM is thus a rather "old" code developed already in the 1970s. The local version of ROMS we use is one which is run by the Institute of Marine Research (IMR) in Bergen, Norway. It is a modern code in all respects and was implemented by IMR just a few years ago (*Budgell*, 2005). Finally, the local version of HYCOM we use is the one employed by the Nansen Environmental Research Center/Mohn Sverdrup Center in Bergen, Norway in their TOPAZ ocean prediction system (*Evensen and Szabo*, 2002; *Laurent et al.*, 2004). HYCOM differs from MIPOM and ROMS in that it employs a hybrid vertical coordinate which is a geopotential depth coordinate near the surface and an isopycnic vertical coordinate at depth. Like ROMS also HYCOM is a modern code.

The simulations are part of the industry-funded project CONMAN (COmparison of Numerical ocean Models Applied to Norwegian waters) with the particular aim of assessing whether ROMS or HYCOM can replace MIPOM for numerical ocean "weather" prediction at **met.no** in Norwegian waters. Ocean weather is connected to eddies, jets and meanders, with a typical length scale of order 10 km in Norwegian waters. These features are responsible for most of the known high current events in these waters. As such they are important events to take into account when designing offshore installations or when performing marine operations. Hence they are important features to simulate correctly at least in a statistical sense.

We run the models for a three year period commencing October 1, 2003 and for a domain covering an area of the northeastern Atlantic Ocean, often referred to as the Atlantic Margin. All models employ a grid size of approximately 4 km, and care is exercised in making the forcing (e.g., atmospheric input, river discharges, topography, initial conditions, lateral open boundary forcing, etc.) as similar as possible. Differences are nevertheless unavoidable. For one, ROMS and HYCOM were run with different lateral boundary forcing, referred to as EKASC and TOPAZ, respectively, while MIPOM was run with both. As such, the MIPOM/TOPAZ and HYCOM simulations are directly comparable as are the MIPOM/EKASC and ROMS simulations, but some care is required in comparing the ROMS and HYCOM simulations.

We analyze results from the period January 1, 2004 through September 30, 2006, following a three month spin-up. We focus on velocities for comparison with in situ measurements at the Svinøy section. As the observations generally do not overlap in time with the model simulations and as there may be significant year to year variability in the currents, we focus on *statistical* comparisons using long time series (preferably longer than two years). This is also sensible in light of the active, small scale eddy field. We first examine the spatial structure of the velocity means and standard deviations, at different depths. Then we present a more

detailed statistical comparison of the data at Svinøy.

The model mean flows and standard deviations are broadly similar in structure. However, there are differences in magnitudes, with ROMS usually more energetic in both measures than MIPOM, and MIPOM more energetic in turn than HYCOM. In addition, MIPOM exhibits an equatorward mean flow beneath the poleward warm inflow from the North Atlantic. HYCOM exhibits a similar flow, but much weaker. ROMS is the only model which exhibits a poleward mean flow at all depths in the inflow. Furthermore, the ROMS inflow bifurcates with the majority of the flow proceeding along the shelf break and with a smaller portion flowing into the North Sea. Also HYCOM bifurcates, but with the majority of the inflow flowing into the North Sea. In contrast the mean flow in MIPOM basically entirely flows into the North Sea, mixing with the Norwegian Coastal Current and thereby altering the water mass characteristics. The observations suggest this is not happening in reality, and thus the ROMS bifurcation is the most realistic one.

The results at Svinøy indicate that the MIPOM and HYCOM fields are consistently too weak compared to the observations, while the ROMS velocities are closer to observed. In fact, the ROMS velocities are actually too energetic in certain locations. Curiously MIPOM velocities are consistently equatorward at depth, as opposed to the ROMS and observed velocities which are nearly always poleward. Overall the directions are better respected by HYCOM than by MIPOM, in particular at the deeper locations, but also HYCOM shows a higher tendency for equatorward flows at depth than indicated by the observations.

The success of the ROMS model in simulating the observed fields derives in part from its use of the third order horizontal advection scheme combined with a better vertical resolution and a more sophisticated numerical handling of the vertical processes. Use of the higher order advection scheme makes ROMS effectively less viscid, implying its effective resolution is higher than MIPOM and HYCOM for the given grid size. The result is an increase in the eddy activity. Thus the likelyhood of capturing more high current events increases. This conclusion is underscored by, e.g., *Winther et al.* (2007) who reported that replacing the second order scheme in HYCOM with higher order advective schemes resulted in higher eddy activity at the same grid resolution. In addition, higher order schemes are better at preserving small scale eddies, which in turn are so important for high velocity events. This is likely why the higher end of the velocity distributions are better captured by ROMS than the other models.

Using higher vertical resolution implies that ROMS has a better representation of the bottom topography. In addition its more sophisticated handling of the vertical processes produces more realistic upslope velocities. Taken together this may explain why ROMS is the only model giving a consistent poleward flow towards Svinøy at all depths.

The use of more sophisticated numerical methods and a higher vertical resolution however has a price. It increases the computer time by a factor of two to three. Optionally to increase the eddy activity, and thereby the eddy kinetic energy in HYCOM and MIPOM, the grid size could be decreased to say 2 km. However, the cost then is to increase the computer time by a factor of eight. Thus we find that use of sophisticated numerical methods is a far better option than increasing the horizontal resolution. Based on these results, we therefore recommend using ROMS as the main operational model for ocean weather predictions at **met.no** to replace MIPOM.

J. A. Johannessen (personal comm.) asked during the initial presentation of these results

how we would do the study differently, if we had the opportunity. If this were to occur, we believe that all the models should be run by a single institution, with identical forcings and set-ups (e.g., the same number of vertical layers and horizontal domains). The present study as it stands could not unfortunately be published in most journals because of the differences in model set-ups. We are very interested in conducting such a study, given the present results.

Contents

List of Tables

List of Figures

1 Introduction

Features such as mesoscale eddies, fronts and jets are responsible for most of the known extreme current events in the ocean. Hence an accurate description of these features is essential to any ocean weather[2] forecasting system. Any ocean prediction system aiming at forecasting these events should therefore be able to predict the wings of the statistical velocity distribution.

At the Norwegian Meteorological Institute (**met.no**) we have for the last 15 years or so used a local version of POM (*Blumberg and Mellor*, 1987) named MIPOM to forecast ocean circulation. It has been upgraded and refined over the years (*Engedahl*, 1995b; *Engedahl et al.*, 2001; *Røed and Fossum*, 2004) and is now **met.no**'s main operational numerical ocean prediction model for forecasting of ocean variables. It produces up to 60 hours forecasts once a day year round for Norwegian waters, and includes nested model regions with eddy resolving capabilities[3]. MIPOM is an 'old' code dating back to the 1980s, and is best characterized as a terrain-following coordinate model. In many respects MIPOM gives valuable and accurate predictions, in particular in a statistical sense (*Martinsen et al.*, 1995; *Engedahl and Røed*, 1999; *Hackett and Engedahl*, 2000; *Jenkins et al.*, 2001; *LaCasce and Engedahl*, 2005). However, recently more modern codes and models of different architecture and characteristics have been developed, and we feel that it would be valuable to compare MIPOM with some of the more modern codes. This is the rationale behind CONMAN[4] which overall aims at providing the best possible ocean model system for operational forecasting of ocean circulation variables in Norwegian waters.

With this in mind we have compared the results from three eddy permitting numerical ocean models of different characteristics and architecture. Specifically we have assessed the results from a three year simulation using MIPOM and local versions of the publicly available models ROMS (Regional Ocean Modeling System, *Shchepetkin and McWilliams*, 2005) and HYCOM (Hybrid Coordinate Ocean Model, *Bleck*, 2002) with the aim of evaluating whether one or both would be a better choice than MIPOM for ocean weather prediction in Norwegian waters. The local version of ROMS, which also may be characterized as a terrain-following coordinate ocean model, is run by the Institute of Marine Research (IMR) in Bergen, Norway (*Budgell*, 2005). The local version of HYCOM conforms to the version run by the Mohn Sverdrup Center (MCS, affiliated with the Nansen Environmental and Remote Sensing Center), Bergen, Norway, and is used for instance in their TOPAZ ocean forecasting system[5]. It utilizes a hybrid depth coordinate consisting of density surfaces (isopycnals) coupled with geopotential coordinates near the surface (*Chassignet et al.*, 2003; *Laurent et al.*, 2004).

The success of any numerical simulation often depends directly on the overall model architecture. This dependence has led to many comparison experiments of which the MOMOP exercise (*Røed et al.*, 1995; *Hackett et al.*, 1995), the EU project DYNAMO (*Willebrand et al.*, 2001), the DAMÉE in the US (*Chassignet et al.*, 2000) and recently the national Norwegian experiment MONCOZE (*Johannessen et al.*, 2006, 2007) are examples. Here we focus on

[2]The term 'weather' is used since the mesoscale eddies, jets and fronts are the oceanic counterpart to the atmospheric cyclones. In Norwegian waters these features typically have a length scale of order 10 km.

[3]Daily updates are available at http://met.no/kyst_og_hav/havvarsel.html

[4]COmparison of Numerical ocean Models Applied to Norwegian waters

[5]Available at http://topaz.nersc.no/

comparing the models in a statistical sense. This is done since the current observations available to us from the Svinøy section (*Orvik et al.*, 2001; *LaCasce*, 2005) and other measurements made by oil companies in the area do not necessarily overlap in time with the three year model simulations. Since there may be significant year to year variability in the currents we focus on long time series. This basically limited us to the Svinøy data, since they are generally longer than two years (longer time series exist at Ormen Lange, but these were not available to us at the time of the analysis). Moreover, since the models velocity distributions and the wings of these distributions are important for establishing the design currents, we focus in particular on how good the models are at capturing the higher end of the velocity distributions.

In an earlier work (*Røed*, 2006) we reported on the set-up of the models and an initial comparison of the three models in the operational phase of CONMAN. Since the set-up in this second phase is slightly different, we start by describing the common configurations chosen for this hindcast phase (Section 2), that is, computational domain, topography, atmospheric input, lateral boundary forcing, etc. Since all the models are continuously upgraded (in part due to the results of the operational comparison exercise described in *Røed*, 2006), we briefly describe the new versions of the models in Section 3. At the end of each model subsection we list some important facts that the reader should keep in mind while reading the analysis part found in Section 4 and the discussion part found in Section 5. Finally, Section 6 offers a summary and presents the recommendations.

2 Common configuration of the models

In setting up the models for the three year simulation care was exercised in making all input as similar as possible. This includes the computational domain and the topography (Figures 1 and 3). Other important input is mesh size, atmospheric driving forces (momentum, freshwater and heat fluxes), input from rivers, tidal forcing, initial conditions and lateral forcing at open ocean boundaries.

The computational domain and area of interest to CONMAN is displayed in Figure 1 and is often referred to as the Atlantic Margin. The area exhibits many topographic features such as the Iceland-Faroes Ridge ($\sim$ 500m deep), the Faroes Bank Channel ($\sim$ 800m deep) and Faroes-Shetland Channel, the Norwegian Basin ($\sim$ 4000m deep) and the Norwegian Trench. The latter cuts into the Skagerrak and reaches depths of $\sim$ 700m. The upper water layers are dominated by the inflow from the south of warm and salty water masses of Atlantic origin through the Faroes-Shetland Channel and the inflow of Polar water from the northwest along and north of the Iceland-Faroes Ridge as displayed by the satellite image in Figure 2. Furthermore the coastal water masses in Skagerrak and along the Norwegian coast are dominated by the outflowing brackish Baltic Water comprising the fresh and (in winter) cold Norwegian Coastal Current (NCC).

As displayed in Figure 2 the surface water masses are separated by sharp fronts: the Iceland-Faroes front along the Iceland-Faroes Ridge, the Polar front extending northeastward from the Faroes towards Spitsbergen, and the front separating the warmer water masses of the inflowing Norwegian Atlantic Current from the NCC flowing along the Norwegian coast. These fronts are unstable (*Fossum*, 2006; *Albretsen*, 2007) and the CONMAN area is therefore a region of

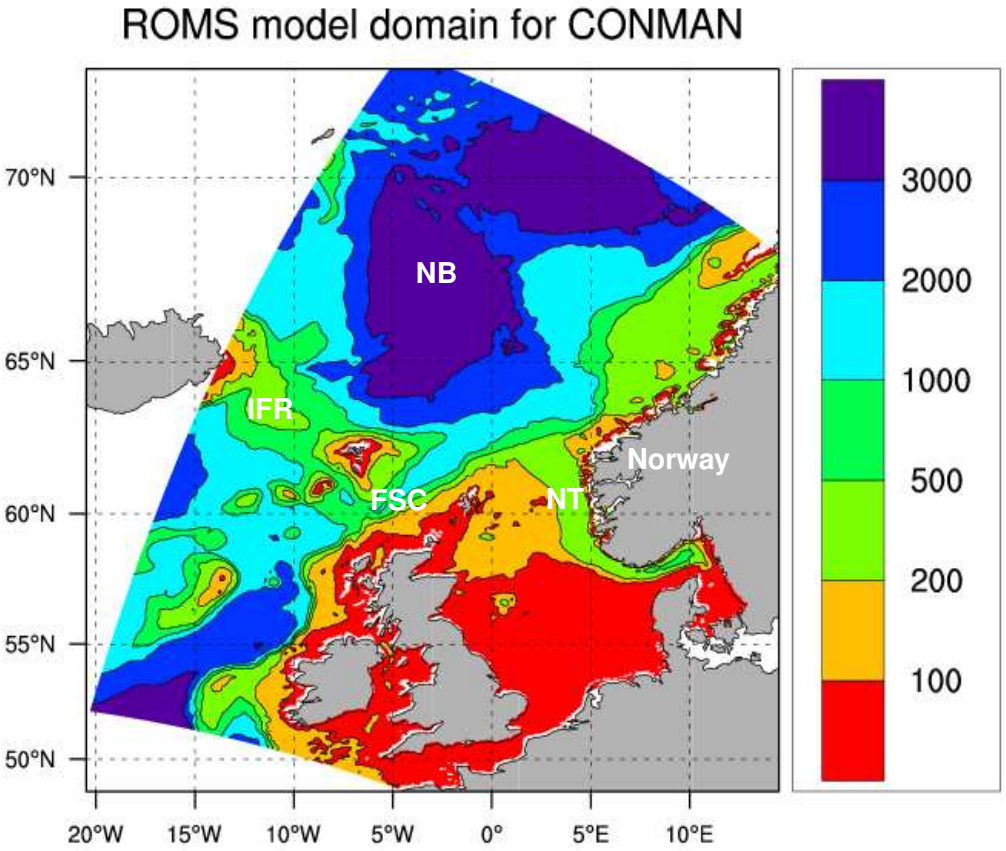

Figure 1: The bottom topography of the CONMAN area. Contours are at 100, 200, 500, 1000, 2000 and 3000 meters. Note the many topographic features including the Norwegian Trench (NT), the Faroes-Shetland Channel (FSC), the Iceland-Faroes Ridge (IFR) and the Norwegian Basin (NB). Displayed is the bottom topography of the 4 km fine mesh domain of the model ROMS. See also Figure 3.

complex dynamics, with many mesoscale features such as eddies, fronts and jets present (Figure 2, right panel). As argued by *Fossum and Røed* (2006), *Fossum* (2006) and *Albretsen* (2007) these structures are dynamically similar to the cyclone systems found in the atmosphere, and are caused by a combination of baroclinic and barotropic instabilities. Moreover they are associated with strong velocities and, as is well known, constitute a potential threat to any marine operation.

The set-up for the hindcast run is similar to the operational set-up described in *Røed* (2006). Thus the mean mesh size is approximately 4 km for all models, but the maximum and minimum grid size (Table 1) differ slightly from model to model due to utilization of different map projections. As shown by Figure 3 this also causes the computational domain to be different (for details see next section). Note that the relative fine mesh of 4 km makes the models eddy

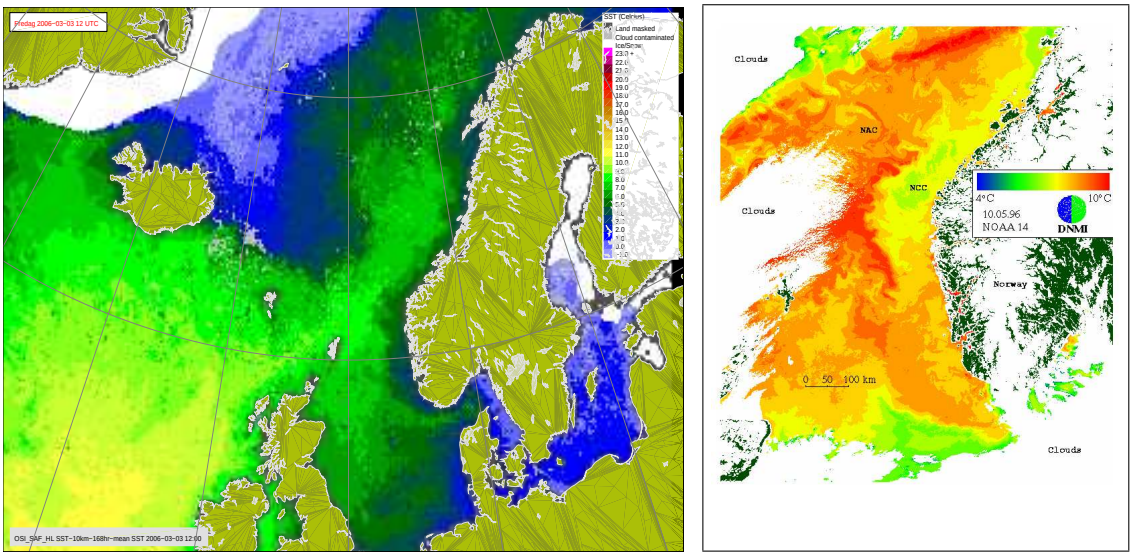

Figure 2: Satellite images depicting the sea surface temperature (SST) in the northern North Atlantic (left panel) and west of Norway (right panel). Left panel shows a one week composite centered on March 3, 2006, with a contour interval of 1°C. The image in the right panel is a high resolution snapshot from May 10, 1996 with a color scale ranging from 4-10 °C. Note the many mesoscale eddies, meanders and jets present. The length scale shown in the middle gives an estimate of the length scale of the mesoscale features, that is, about 10 - 30 km.The abbreviations used are NCC: Norwegian Coastal Current and NAC: Norwegian Atlantic Current. This and similar images are available at http://saf.met.no/.

permitting[6]. The three year simulation commenced on October 1, 2003 00UTC and ended on October 31, 2006 00UTC.

The bottom topography was prepared by H. Engedahl and Jon Albretsen at **met.no** and is derived from the etopo2.5 (2.5' latitude-longitude resolution) with additional data from various local sources. The necessary atmospheric variables to derive momentum, heat and freshwater fluxes are extracted from the operational analysis at ECMWF (European Centre for Medium-Range Weather Forecasts) as described in *Røed* (2006). Regarding freshwater input from rivers all models use climatological monthly mean values prepared by Jon Albretsen, **met.no** (*Røed*, 2006).

The computational domain has large open boundaries to the south, west and north, at which lateral open boundary conditions are imposed. For reasons explained in Section 4 we have used two sets of boundary values as lateral forcing. The first is prepared by Laurent Bertino and Cecilie Hansen at MSC and consists of daily mean values of water level (no tides), currents and hydrography (henceforth referred to as TOPAZ boundary forcing). It is based on a run with an extended coarser resolution, basin wide version of HYCOM that covers all of the

[6]the phrase eddy permitting is used to acknowledge that although the models do resolve an eddy once it is formed they do not necessarily resolve all processes that cause mesoscale features in general and eddies in particular to be created.

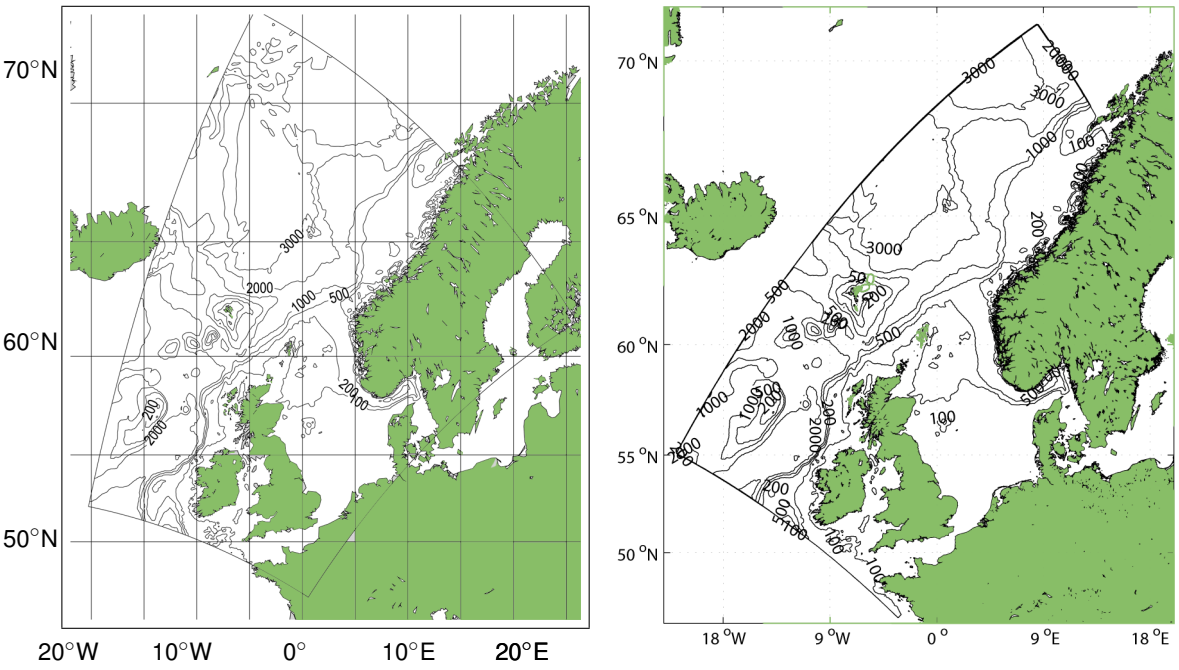

Figure 3: Computational domain and topography of MIPOM and ROMS (left panel) and HYCOM (right panel). Contours are at 100, 200, 500, 1000, 2000 and 3000 meters. Note the difference in map projection which gives rise to differences in the computational domain covered by ROMS/MIPOM compared to HYCOM.

northern hemisphere Atlantic Ocean and part of the South Atlantic ocean (Figure 4, right panel). This area is the same as that covered by the TOPAZ2 system at MSC. The basin wide version of HYCOM used for this purpose is however different from the HYCOM version used in the TOPAZ2 system. The second set consists of climatological monthly mean values of the same variables extracted from the EKASC archive (*Engedahl et al.*, 1997) (henceforth referred to as EKASC boundary forcing) covering a much smaller area (Figure 4, left panel). Note that none of the two sets of lateral boundary values include tides. Tidal elevation and tidal currents are therefore specified separately as described in *Røed* (2006). Also note that the domains covered by the two sets of lateral boundary values, although different, wholly encompass the fine mesh areas depicted in Figure 1.

We emphasize that although each of the individual inputs described above are equal, each model use a different formula to convert these inputs to specific model forcing. For instance the momentum input to the model is in the form of a surface stress (or wind stress), while the specified input is the atmospheric 10 m wind speed and direction. The input is therefore converted to wind stress using a formula or parametrization specific to each model. As a consequence the wind stress applied in each model may differ even though the 10 m wind speed and direction is the same. The same is true for the other inputs like lateral boundary forcing, river discharges, heat fluxes and tidal forcing. All of these conversion formula are hence an inherent part of the model code just like the numerical schemes utilized for internal processes

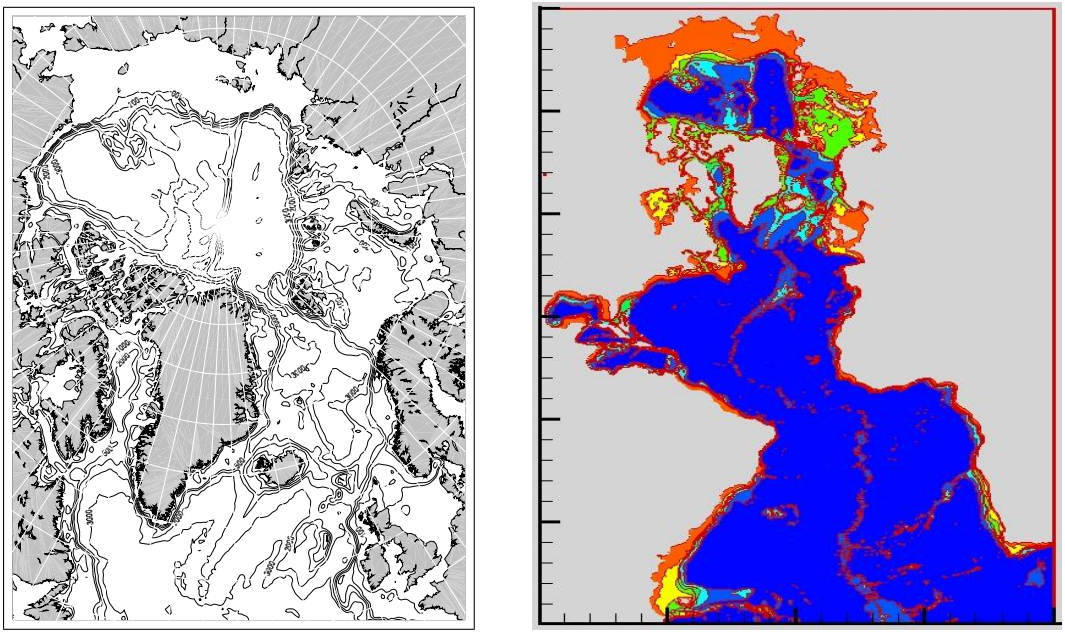

Figure 4: EKASC area (left panel) and TOPAZ area (right panel) with depth contours at 100 m, 200m, 500 m, 1000 m, 2000 m and 3000 m.

such as, e.g., mixing and advection. It should therefore be kept in mind that differences in the various conversions may give rise to differences in the model results on an equal basis as differences in the choice of numerical schemes used to integrate the model equations forward in time and space.

3 Characteristics of the models

All three models MIPOM, ROMS and HYCOM are described in some detail in *Røed* (2006). Here we focus on what is new and on specific model details of importance for this comparison. We remind the reader that the main differences between the MIPOM and ROMS architecture on the one hand and the HYCOM architecture on the other hand is that the two former models utilizes a terrain-following vertical coordinate while the latter uses a hybrid vertical coordinate. Terrain-following implies that the vertical levels follow the bottom contours and transform the depth coordinate from a depth coordinate to a non-dimensional vertical coordinate, commonly denoted σ, which then has the range $\sigma \in [-1,0]$. The hybrid vertical coordinate in HYCOM consists of the normal geopotential depth coordinate near the surface while transforming the governing equations to an isopycnic coordinate system for the layers further down. For a detailed description of vertical coordinate systems in general, and the two mentioned here in particular, we refer the reader to *Griffies* (2004, Chapter 6). One consequence of this difference in vertical coordinate system is that HYCOM has less vertical resolution (less layers) in shallower areas than the terrain-following models.

Table 1: Model facts

Text	Unit	MIPOM	ROMS	HYCOM
Mean mesh size	*m*	4046	4046	≈ 4000
Maximum mesh size	*m*	4340	4340	4054.55
Minimum mesh size	*m*	3830	3830	3967.38
No. of vertical levels/layers	-	26	32	22
Horizontal dissipation	-	Smagorinsky[1]	No explicit diffusion[2]	Smagorinsky + FCT[3]
Vertical mixing	-	Mellor-Yamada 2.5 level[4]	GLS mixing scheme[5]	KPP mixing scheme[6]
Mode splitting	-	yes	yes	yes
Horizontal advection scheme	-	2nd order centered	3rd order upwind	2nd order centered
Long (internal) time step	*s*	180	120	100
Ratio of internal to external time step	-	36	30	10

[1] *Hackett and Røed* (1994, page 117), [2] There is some weak horizontal diffusion due to the application of the third order upwind advection scheme, [3] *Bleck* (2002), [4] *Galperin et al.* (1988), [5] *Umlauf and Burchard* (2003), [6] *Large et al.* (1994)

Other obvious differences between the models are revealed in Table 1. Deviations from the common configuration as described in Section 2 are documented if necessary.

3.1 MIPOM

The MIPOM model version we use is upgraded from the one used in the operational phase, in particular in the way the atmospheric forcing is converted to model input. The latter is now in accord with *Røed and Debernard* (2004). The mesh sizes and number of vertical, terrain-following, levels are given in Table 1. We use levels that are unevenly spaced with the highest resolution at the top. The σ-levels are (multiplied by -1000) at 0, 2, 5, 10, 20, 35, 50, 75, 100, 125, 150, 175, 200, 250, 300, 350, 400, 450, 500, 550, 600, 700, 800, 900, 950 and 1000, respectively. Thus at 1000 m depth the actual depth in meters are found by multiplying each number with -1. For bathymetry we use the topography file provided by Jon Albretsen at Norwegian Meteorological Institute. The simulations with MIPOM is completed on the new massive parallel supercomputer platform at NOTUR named Njord (http://www.notur.no/hardware/njord/). Specifically we use 16 CPU units each consisting of 8 nodes (a total of 128 nodes).

A leapfrog (second order, centered in time and space) combined with an Asselin filter to damp the unphysical mode is used both in the momentum, salinity and heat equation for the horizontal advective part. For the vertical advection a first order (forward in time) upwind scheme is used. For the vertical mixing MIPOM uses a second order turbulence closure scheme

as described in *Mellor and Yamada* (1982) with minimum values for the parameters as given in Table 1. Horizontal diffusivity for momentum and heat/salinity are included to damp small scale computational noise. It depends on the horizontal velocity shear and on the horizontal grid spacing according to *Smagorinsky* (1963) (for numbers used see Table 1).

To convert the lateral boundary values specified at the open boundaries (nesting condition) we use the well known Flow Relaxation Scheme (FRS, *Martinsen and Engedahl*, 1987). All rivers are treated as point sources of fresh or brackish water released at a single model grid point. The fresh water is mixed over the entire water column at the outlet grid point, according to a vertical distribution (maximum flux at the surface and zero flux at the bottom).

As mentioned is the conversion of atmospheric input to fluxes at the surface now via a separate module integrated with a sea ice model (*Røed and Debernard*, 2004). Hence MIPOM is now equipped with a sea-ice model module. The net radiative flux, i.e., the sum of solar and net longwave radiation and the sensible and latent heat transfer, is calculated in the separate module and used in the ocean model as the surface boundary condition for heat flux. A surface condition for the freshwater (salinity) flux is specified by the difference between precipitation and evaporation. During 2005 and 2006 the heat fluxes were relaxed (via a crude assimilation/nudging scheme) to SST-analysis. The SST analysis is derived merging OSISAF SST (http://saf.met.no) with the ECMWF SST-analysis.

Bottom stress follows the formulation of *Gerritsen and Bijlsma* (1988), that is,

$$\tau_b = C|\mathbf{u}_b|^2\mathbf{u}_b \tag{1}$$

where τ_b is the bottom stress, $\mathbf{u}$ is the bottom velocity and C is a constant dependent on the equilibrium depth (decreases with increasing equilibrium depth).

Tides are applied to the model by specifying amplitude and phase of sea level and depth-mean currents along the open boundaries. Eight dominant tidal constituents are included: four semi-diurnal (M_2, S_2, N_2 and K_2) and four diurnal (K_1, O_1, P_1 and Q_1). The amplitude and phase information for these constituents are obtained from the numerical simulations of *Flather* (1981) and *Gjevik et al.* (1990, 1994).

The vertically integrated equations (external mode) are separated from the vertical structure equations (internal mode) by mode splitting. This technique permits calculation of a free surface elevation by solving the velocity transport[7] separately from the three-dimensional velocity and hydrography. The external mode portion of the model uses a short time step based on the common CFL condition for numerical stability using the external wave speed as input, while the internal mode uses a long time step based on the internal wave speed as input. The internal time step used is 180 seconds, while the external time step used is 5 second, that is a ratio of 36.

Important facts to remember about the MIPOM simulation:

- Assimilation of an SST analysis for the last two years.

[7]The velocity transport is simply the depth mean velocity multiplied by the depth of the water column.

- Two runs performed, one with TOPAZ at the lateral boundaries (henceforth referred to as the MIPOM/TOPAZ simulation, and one with EKASC at the lateral boundaries (henceforth referred to as the MIPOM/EKASC simulation).

3.2 ROMS

The version of ROMS we use is upgraded from version 2.1 to 3.0 with extensions from IMR. The main reason for the change is to take advantage of the reworking of the ROMS tidal formulation at IMR, including the nodal correction. The latter fixes the phase error of the previous version prominent in the operational products (*Røed*, 2006). The mesh sizes and number of vertical levels are given in Table 1. The mesh size is equal that of MIPOM, while the number of vertical levels are larger then MIPOM. Also the bathymetry used equals that of MIPOM. Like the MIPOM simulations also the ROMS simulation was completed on the new supercomputer Njord, utilizing the same number of nodes and CPU units. In fact it was run by people at the Norwegian Meteorological Institute with help from IMR.

The depth coordinate is the generalized terrain-following vertical coordinate described in *Song and Haidvogel* (1994). The advantage of the generalization is that it allows us to simultaneously maintaining high resolution in the surface layer as well as dealing with steep and/or tall topography. Depth of levels can be calculated using the *s*-coordinate formula of *Song and Haidvogel* (1994) with $\theta_s = 3$, $\theta_b = 0.8$ and $hc = 5$. At a depth of -1000 meters the levels are at (from bottom and up) -991, -972, -953, -932, -909, -884, -858, -828, -796, -761, -722, -681, -638, -592, -544, -496, -447, -399, -352, -307, -265, -226, -190, -158, -129, -103, -81, -61, -44, -29, -16, -5 meters, respectively.

ROMS has a wide variety of advection schemes of relative high order. Here we use a 3rd order upwind biased scheme for the horizontal advection of momentum, salinity and temperature (*Shchepetkin and McWilliams*, 1998). In our experience this scheme has good properties in maintaining fronts and permitting mesoscale eddies and filaments. In the vertical the parabolic spline-based representation of *Shchepetkin and McWilliams* (2005) and *Haidvogel et al.* (2007) is used. This scheme gives effectively a very high order vertical advection. ROMS also offers several vertical mixing schemes. The one used here is the two-equation $k-\omega$ scheme of the Generic Length Scale (GLS) formulation of *Umlauf and Burchard* (2003). The implementation of this scheme in ROMS is documented in *Warner et al.* (2005). Note that no explicit horizontal diffusion is used. As displayed in Table 1 we emphasize that although no explicit horizontal diffusion is employed in ROMS, the 3rd order upwind scheme provides some implicit diffusion. The vertical diffusion is embedded in the GLS scheme.

A variety of open boundary schemes are available in ROMS (*Marchesiello et al.*, 2001). Here we use the Flow Relaxation Scheme (FRS, *Martinsen and Engedahl*, 1987)) for salinity, temperature and baroclinic currents (internal mode), while we use a combination of the *Chapman* (1985) and the *Flather* (1976) conditions for the external mode, that is, for the sea surface deviation and the vertical integrated transport (*Ådlandsvik and Budgell*, 2003). The same river locations and discharges as in MIPOM are used. In ROMS we implement the rivers as a volume flux across the land-sea boundary. A vertical profile is used, giving highest flow in the upper *s*-levels.

To convert atmospheric values to a momentum and heat flux input to the model we use

the standard ROMS bulk flux routine as described in *Fairall et al.* (2003) implementing the COARE algorithm. The bottom friction is quadratic and follows (1) with a coefficient of $3.0 \cdot 10^{-3}$ (Table 1).

The tidal forcing of ROMS has been reimplemented at IMR, including tidal potential (not used in CONMAN) and nodal correction. Both tidal elevation and depth integrated current is included in the boundary forcing by the aforementioned Chapman/Flather boundary condition which is designed for this purpose. As in MIPOM we use a mode splitting to separate the external and internal modes in ROMS. It is a fairly advanced and recently developed scheme in particular regarding the exchange of information between the modes (*Shchepetkin and McWilliams*, 2005; *Haidvogel et al.*, 2007). The actual time step we use is 120 seconds for the external mode, and with a ratio of 36 between external and internal time step (Table 1).

Important facts to remember about the ROMS simulation:

- Advection scheme is third order.
- No explicit horizontal viscosity and diffusion.
- Only run with EKASC as lateral boundary forcing.
- No data assimilation or relaxation is used.

3.3 HYCOM

The main upgrade for this Phase 2 is that the nesting-routines (open boundary condition) for the barotropic part (external mode) is corrected and that new viscosity-parameters are specified. The latter means less damping due to eddy viscosity. The number of layers in the vertical is 22 with the following target potential densities in each layer (in kg/m^3 and σ_θ units): 21.80, 22.20, 22.60, 23.05, 23.55, 24.05, 24.96, 25.68, 26.25, 26.69, 27.03, 27.29, 27.49, 27.66, 27.80, 27.90, 27.97, 28.02, 28.05, 28.08, 28.10, 28.11. Since some of these are isopycnic layers their depth changes in time and space. Unlike the two other models HYCOM is run by the MSC personnel on the IBM e1350 cluster in Bergen, Norway featuring x86_64 processors (Opteron 250). The number of nodes we use is 10 (divides the CONMAN area in 2x5 areas). We also note that the bathymetry information comes from a different source, but the deviations are small, in particular on the large scale.

The advection scheme we use is a combination of a leapfrog (2nd order, centered in time and space) and FCT (Flux Conserving) scheme. The vertical mixing is the KPP-mixing scheme described in *Large et al.* (1994). The lateral (within layers) mixing schemes we use is, as in MIPOM, the scheme due to *Smagorinsky* (1963). In addition we use the inherent biharmonic viscosity and diffusion schemes implemented in HYCOM. The values used are 0.1 for the deformation-dependent Laplacian viscosity factor, 0.0 for the deformation-dependent biharmonic viscosity factor, 0.005 m/s for the diffusion velocity for harmonic (Laplacian) momentum dissipation and 0.01 m/s for the diffusion velocity for biharmonic momentum dissipation. In addition we use 0.0 m/s for the diffusion velocity for Laplacian thickness diffusion and 0.01

m/s for the diffusion velocity for biharmonic thickness diffusion. We also apply a 'cushion' function to match the isopycnic interior to the near surface z-layers (*Bleck*, 2002).

The nesting condition (open boundary condition) is as described in *Røed* (2006), that is, for the external mode we use the hyperbolic wave equation as described in *Browning and Kreiss* (1982, 1986), while we use the Flow Relaxation Scheme (FRS) for the internal mode (including layer interfaces) as done in MIPOM and ROMS. The atmospheric input is converted as described in *Røed* (2006) and conform to the formula given in *Drange and Simonsen* (1996). To accommodate the river input we specified them as negative salinity fluxes at the surface, in a predefined area of influence given by a radius of 80km. Although we use no assimilation in the nested model, we do apply a weak relaxation to GDEM v3.0 climatological temperature and salinities with a relaxation time scale of 200 days. No bottom friction was applied. The tidal forcing is specified as a barotropic forcing at the open boundaries. Like the other two models we use the eight constituents K_1, O_1, P_1, Q_1, M_2, N_2, S_2 and K_2 and the astronomical tidal argument based on the positions of the Moon, Earth and the perigee of the Moon.

Important facts to remember about the HYCOM simulation:

- Computational domain is smaller (Figure 3)
- Only run with TOPAZ boundary forcing.
- The topography file is slightly different.
- Weak relaxation to climatological temperature and salinities.

4 Analysis

4.1 Boundary forcing

In first analyzing the results, we encountered a problem with the fields from which the boundary conditions were derived. The TOPAZ simulation which we used to provide daily means of temperature, salinity, pressure and currents on the boundaries, was run with too little lateral dissipation (due to an error in the input file). This produced significant grid-scale noise in the velocity fields (not shown), but evidently did not alter the volume fluxes[8]. This was not noticed until after the HYCOM and MIPOM simulations were already completed.

To test the effects of the small-scale noise on the interior velocity fields, we reran MIPOM with boundary fields derived from the EKASC monthly climatology. The latter are generated by using MIPOM with fixed hydrography to produce consistent velocity fields from a given climatology (in this case the Levitus climatology augmented with observations from the Nordic Seas region *Engedahl et al.*, 1997). The fields represent monthly means, and so offer less temporal resolution than the (daily) TOPAZ fields. However they offer a fully consistent barotropic flow component, which is important for the inflows.

[8]Note that these fields were produced exclusively for CONMAN purposes and are not the same as the daily products displayed on the TOPAZ web site.

The results of the twin MIPOM experiments (henceforth referred to as MIPOM/TOPAZ and MIPOM/EKASC, respectively), suggested that the change in boundary conditions primarily affected the flow near the inflow regions (compare for instance the two upper panels in Figure 7). It had a lesser impact in the interior. However, because the relative strengths of the inflow west of Scotland and that north of the Faroes were altered, the strengths of the outer and inner branches of the Norwegian Atlantic Current (NwAC) were also altered. In addition, the eddy kinetic energy associated with the small scale noise in the TOPAZ fields did not appear to penetrate far into the interior. However, because ROMS has higher order advective schemes which are designed specifically to preserve such small-scale features, the penetration of the fictitious eddies could potentially be worse in those simulations.

We therefore decided to run ROMS with the EKASC boundary conditions rather than TOPAZ. The ROMS runs must thus be compared to the MIPOM/EKASC simulations, and the HYCOM runs with the MIPOM/TOPAZ simulations. This is obviously not an ideal situation, but, as will be seen hereafter, the two MIPOM runs are more similar than different.

Hereafter we will compare the models to each other and to various observations. The observations we have generally do not overlap in time with the model simulations, so we will focus on *statistical* comparisons. As demonstrated for instance by *LaCasce and Engedahl* (2005) and *LaCasce* (2005), predictability off the Norwegian coast is relatively low due to the energetic, small scale (order 10 km) eddies there. Accurate current prediction will therefore require widespread data assimilation, but comparing the models with such assimilation would obscure the workings of the models themselves. As the latter is the focus here, a statistical comparison is the most sensible approach. Moreover, since the observations and the model simulations do not overlap in time, and that there may be significant year to year variability in the currents, we also focus on statistics based on long time series, that is, time series longer than two years.

4.2 Means

We consider first the large scale mean velocity fields. The means were generated from daily mean velocities over the model grid and pertain to the period from January 2004 to September 2006. We focus primarily on the means at 50 m depth, but will also show the corresponding fields at 100 and 400 m.

4.2.1 Observations

For observations, we use an estimate of the mean regional surface velocities, derived from the "Rio05" product of the CLS Space Oceanography Division of AVISO. Rio05 estimates the mean dynamic sea surface height for the 1993-1999 period using a multi-variate analysis of hydrographic data, surface drifter velocities and altimetry (the geoid is corrected using both the CLS01 MSS - EIGEN-GRACE 03S geoid and the NOAA (Levitus) WOA98 climatology[9], referenced to 1500 dbar). The geostrophic velocities are then estimated by differencing the sea surface height. We emphasize that the Rio05 fields are based solely on in situ and satellite

[9] http://www.cdc.noaa.gov/cdc/data.nodc.woa98.html

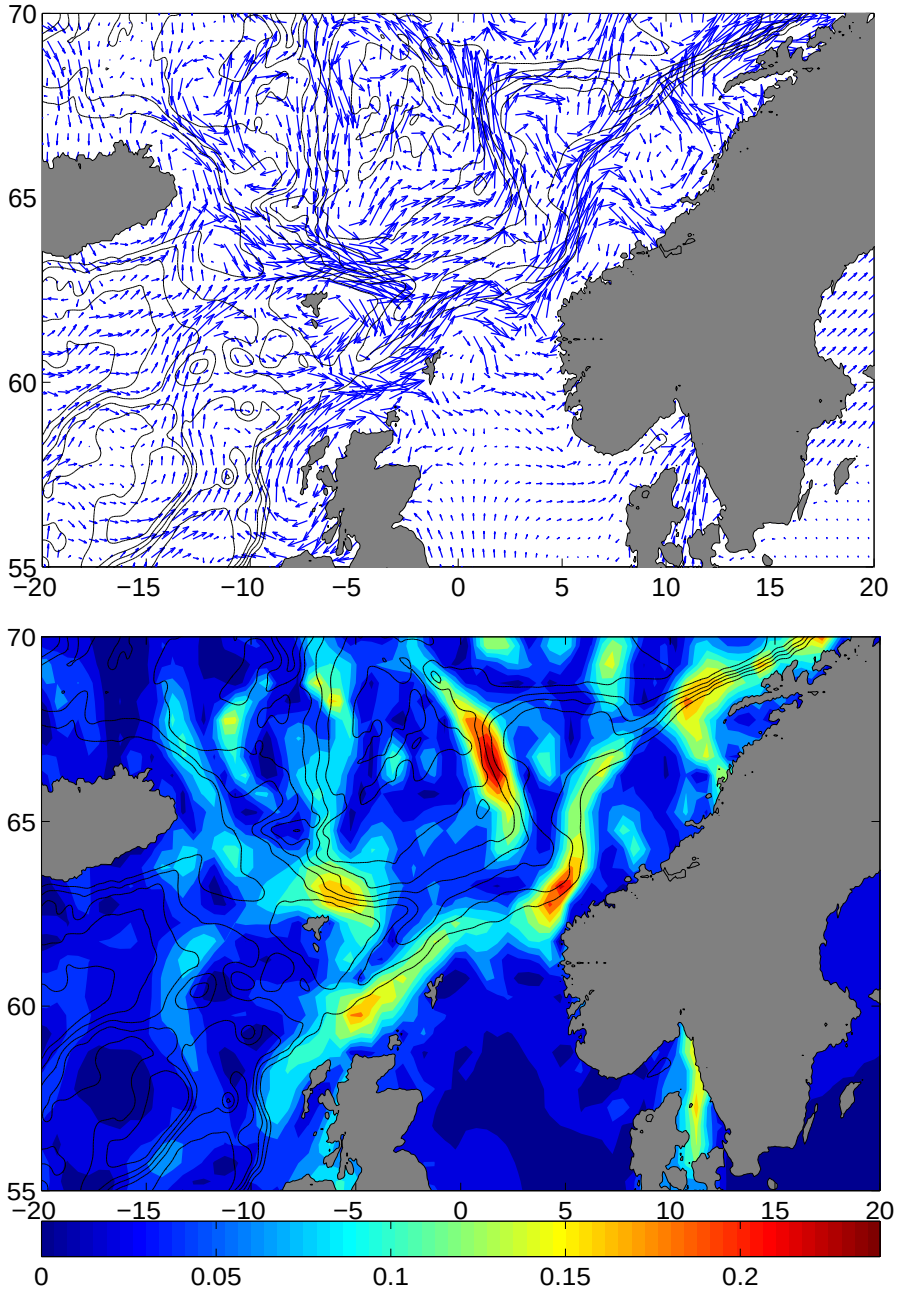

Figure 5: Surface velocities (upper panel) and speeds (lower panel) from the Rio05 product. The velocities correspond to means from the period 1993-1999. The color scale shows speed in m/s.

data, i.e., they do not involve a numerical model. The primary drawback is that the Rio05 fields are calculated on a 50 km grid and thus capture only a smoothed version of the surface flow.

The horizontal velocity vectors and contours of the corresponding speeds are shown in

Figure 5. Despite some unrealistic features (e.g. the flow towards southwestern Sweden and away from the coast of Scotland), the fields are otherwise in line with circulation schemes derived from hydrography (*Mauritzen*, 1996). Of primary relevance here is that there is a strong inflow from the North Atlantic, the NwAC, which enters in two branches, one west of Scotland and the other to the north of the Faroes following the fronts outlined in Section 2.

The "inner branch" tracks the 500 m isobath. A portion peels off to flow into the North Sea, while the majority proceeds off the Norwegian coast, past Ormen Lange. A portion peels off near the Vøring Plateau to join the Norwegian Coastal Current (NCC), and this portion then rejoins the inner branch as it flows toward the Arctic.

The outer branch coincides with the front between the warm inflow and the cooler interior waters in the Norwegian basin (*Mauritzen*, 1996; *Orvik and Niller*, 2002) and approximately follows the 1500 m isobath. It is seen clearly north of the Faroes, as the flow intensifies due to a constriction in the bottom topography. It spreads out thereafter, but strengthens again near the Vøring Plateau. The current then splits, with a portion circulating in the Norwegian gyre and the rest continuing around the plateau, to rejoin the inner branch.

The maximum speeds are on the order of 25 cm/sec. This is a somewhat low value compared to in situ estimates from current meters, which indicate mean speeds of order 40 cm/sec near the surface in the inner branch (*LaCasce*, 2005). The lower speeds here undoubtedly stem from the low resolution of the height fields. We see that the speeds are greatest in regions of topographic constriction, e.g. at Ormen Lange, west of the Vøring Plateau and north of the Faroe Islands.

The mean flow here is important for regional variability. Both the inner and outer branch are known to generate eddies, which spread laterally away from the current cores. In addition, drifter and current meter observations (*Orvik and Niller*, 2002; *LaCasce*, 2005) suggest the outer branch is more time-dependent than the inner one. So the outer branch is more difficult to observe with stationary measurements, like current meters.

4.2.2 Models at 50 m

As an example of the typical model response at 50 m, consider the mean velocity vectors from the MIPOM/EKASC simulation, shown in Figure 6. The Atlantic water flows in west of Scotland and north of the Faroes, and then proceeds northward in two branches. The inner branch begins as expected. However, rather than tracking the 500 m isobath, it follows the 200 m isobath into the North Sea. Here it recirculates and joins the NCC. This differs from the circulation in Figure 5, where only a small fraction of the inner branch makes such a detour. But the inner branch continues thereafter along the shelfbreak through Ormen Lange, as it should. And as in the observations, a portion of the current peels off south of the Vøring Plateau to flow across the shelf, before rejoining the shelfbreak.

The model's outer branch is also clearly visible. However, unlike in the observations, a large portion of the current veers south, east of the Faroes, and joins the inner branch. However the rest continues along the 1500 m isobath and a portion of the inner branch later rejoins this flow. The current thus resembles the observed outer branch by the time it reaches the Vøring Plateau.

We compare the 50 m mean velocities from the different models by examining contours

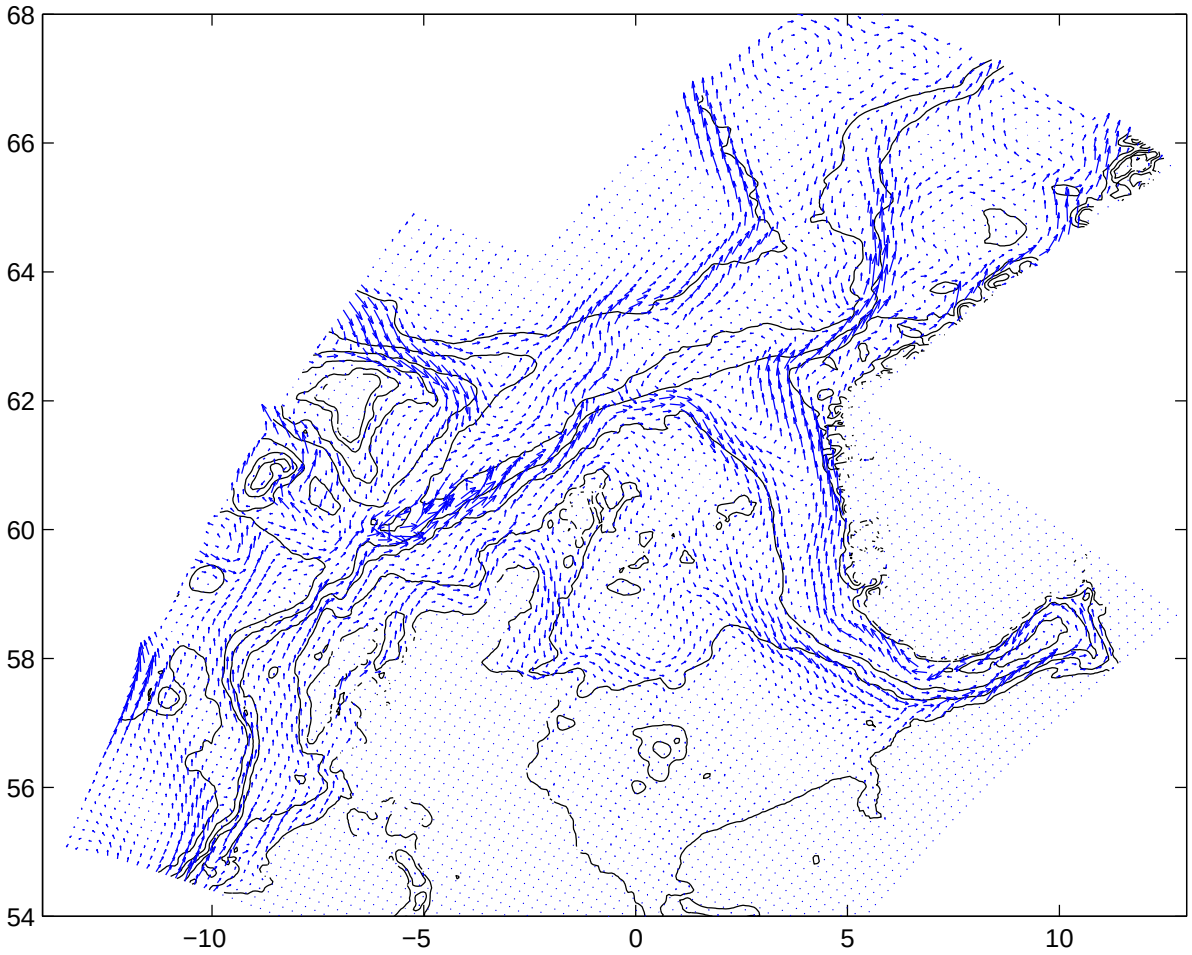

Figure 6: Mean current vectors at 50 m depth from the MIPOM/EKASC simulation.

of the current speed, as in the lower panel of Figure 5. These are shown in Figure 7. The results are plotted over the same region, despite that there are model-to-model differences in the regions where velocities were saved. We employ the same color axes, so that the speeds are directly comparable in the four plots.

The MIPOM/EKASC speeds are shown in the upper right panel of Figure 7. The outer and inner branches of the Atlantic inflow are evident, as is the NCC. The maximum velocities are on the order of 50 cm/sec, with typical speeds of 20 cm/sec. The MIPOM/TOPAZ means (Figure 7 upper left panel) are generally very similar to MIPOM/EKASC means. The differences are that the inflow north of Faroes is weaker and that west of Scotland stronger. This causes the outer branch to be weaker and the inner branch to be somewhat stronger. But the fact that the fields are so similar implies the change in boundary forcing does not induce major changes in the means over most of the region. The HYCOM means are shown in the lower left panel of Figure 7. Recall that the simulation was made using the TOPAZ data on the boundaries. The flow is qualitatively like that in the MIPOM/TOPAZ run, but the HYCOM velocities are weaker,

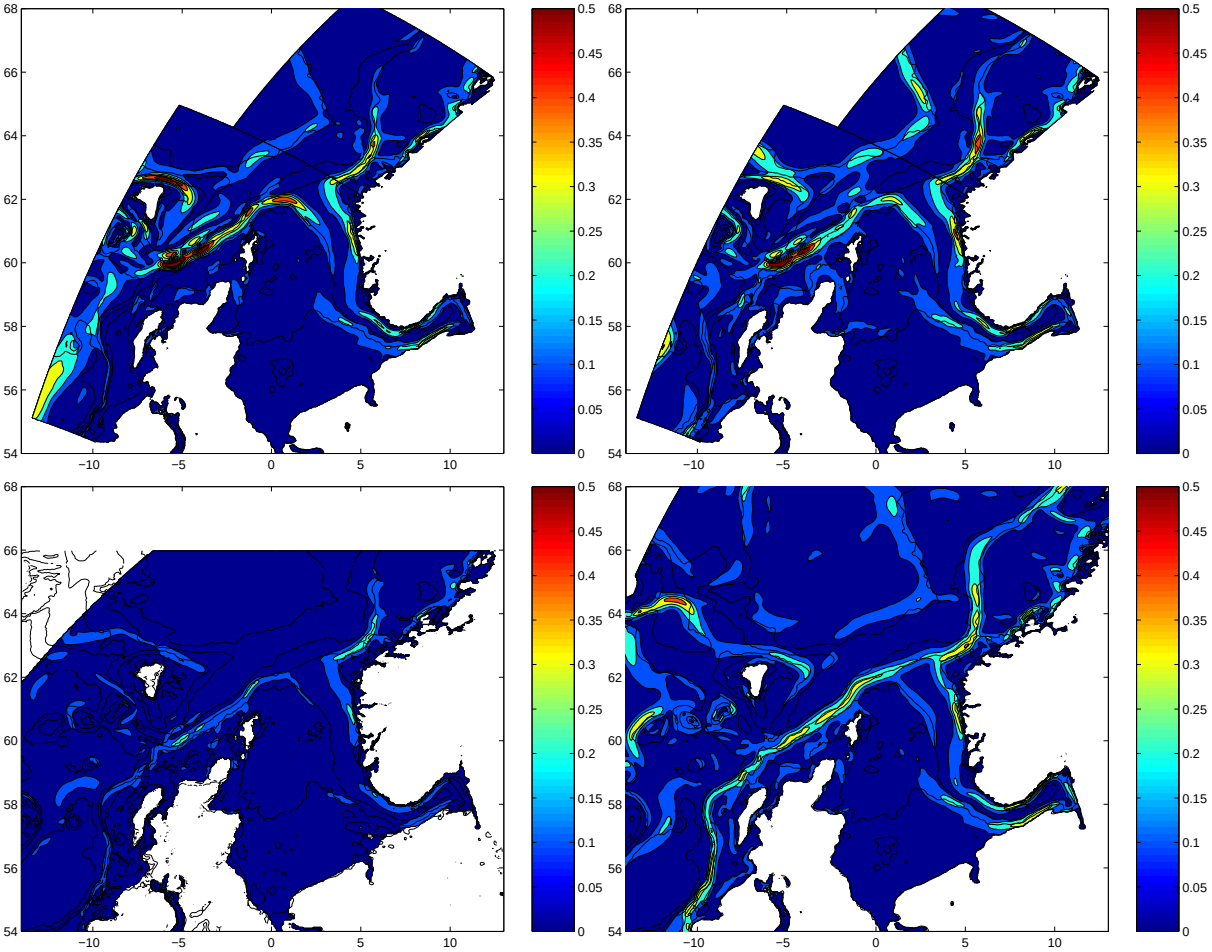

Figure 7: Mean speed contours at 50 m depth from the MIPOM/TOPAZ simulation (upper left panel), the MIPOM/EKASC simulation (upper right panel), HYCOM simulation (lower left panel) and ROMS simulation (lower right panel). The color scale is in units of m/s and ranges from 0 to 0.5 m/s.

by roughly a factor of 2. The inner branch of the NwAC and the NCC are both evident, but the outer branch is much weaker and hence cannot be seen in Figure 7.

The ROMS means (Figure 7) are qualitatively like the MIPOM/EKASC fields, and in most instances the speeds are comparable. The inner and outer branches are seen, as is the NCC. The ROMS outer branch is somewhat weaker than that in the MIPOM simulations. This is due in part to the fact that the current is much more variable in the ROMS model, as seen hereafter. However the ROMS NCC is very similar.

The primary difference with the ROMS means is in the path of the inner branch. As in the MIPOM run, the current tracks the 500 m isobath west of Ireland. But it bifurcates at 62°N, 2°E. Thereafter the majority of the current proceeds northwest while only a fraction peels off and enters the North Sea. This is more consistent with the observations in Figure 5 and with the path inferred from hydrography (*Mauritzen*, 1996). The ROMS model is thus the only one which properly captures this bifurcation.

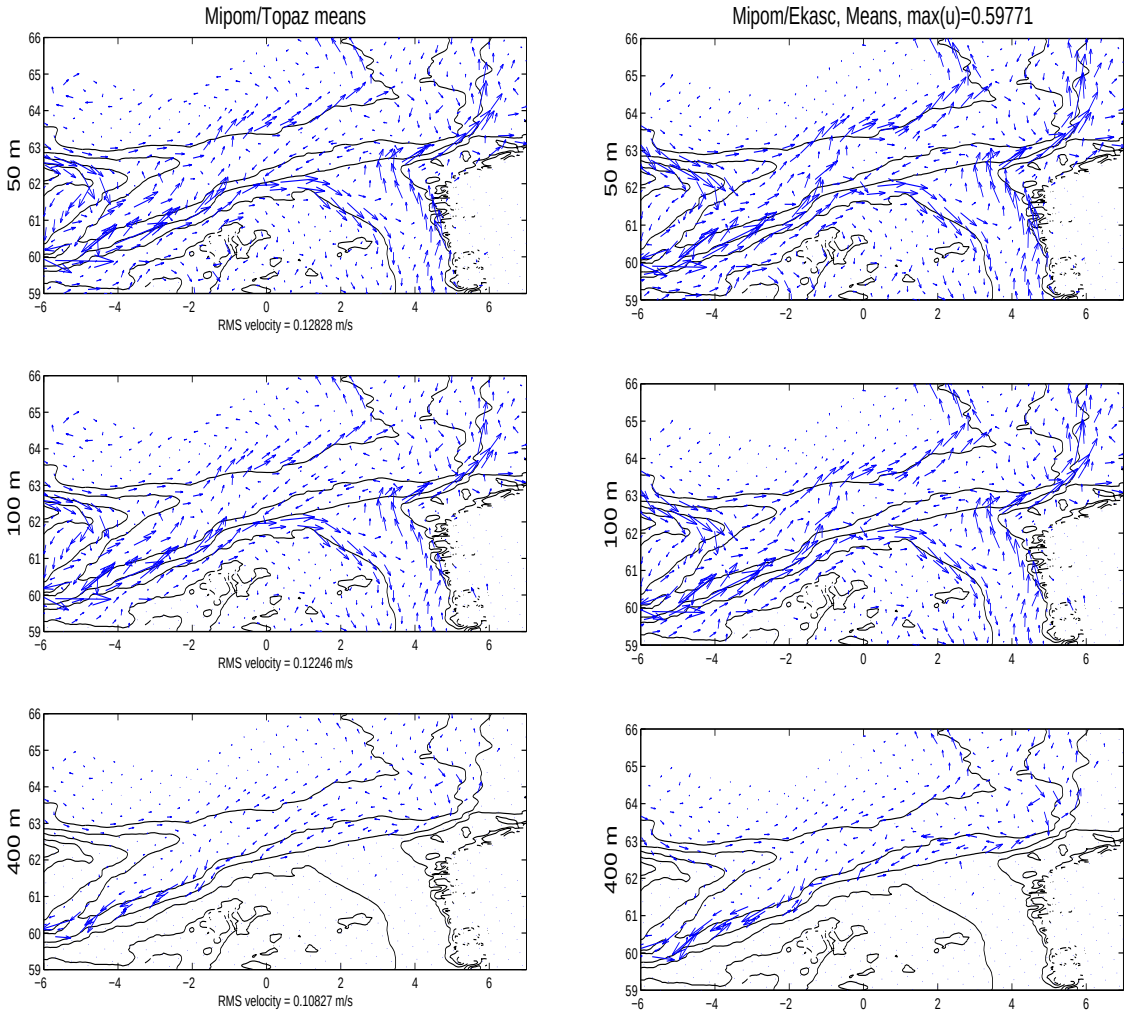

Figure 8: Velocity vectors from the MIPOM/TOPAZ (left panels) and MIPOM/EKASC (right panel) simulation at 50, 100 and 400 m. The rms velocities over the region are shown below each panel

4.2.3 Vertical variation

Next we examine how the means vary in the vertical. In the next two plots, we show velocity vectors at 50, 100 and 400 m depth from the four model runs. We focus here on the region of the shelf and slope off Norway, including Svinøy and Ormen Lange. The vectors are scaled so that the velocities at different depths are comparable. However, the scaling differs between models, so one cannot compare from figure to figure. The rms velocities at each depth for the region are indicated under each panel.

The MIPOM/TOPAZ and MIPOM/EKASC velocities are shown in Figure 8. We see clearly the features described earlier, in particular the detour of the inner branch into the North Sea. The velocities at 100 m depth are nearly the same, albeit slightly weaker. The velocities are weaker still at 400 m. At this depth there is no detour into the North Sea, because the latter is too shallow. The inner branch instead tracks the shelfbreak. But the mean flow is to the *south*, back toward the North Atlantic. This flow reversal in MIPOM has been noted before, by *Engedahl and Røed* (1999), *Hackett and Engedahl* (2000) and *LaCasce and Engedahl* (2005).

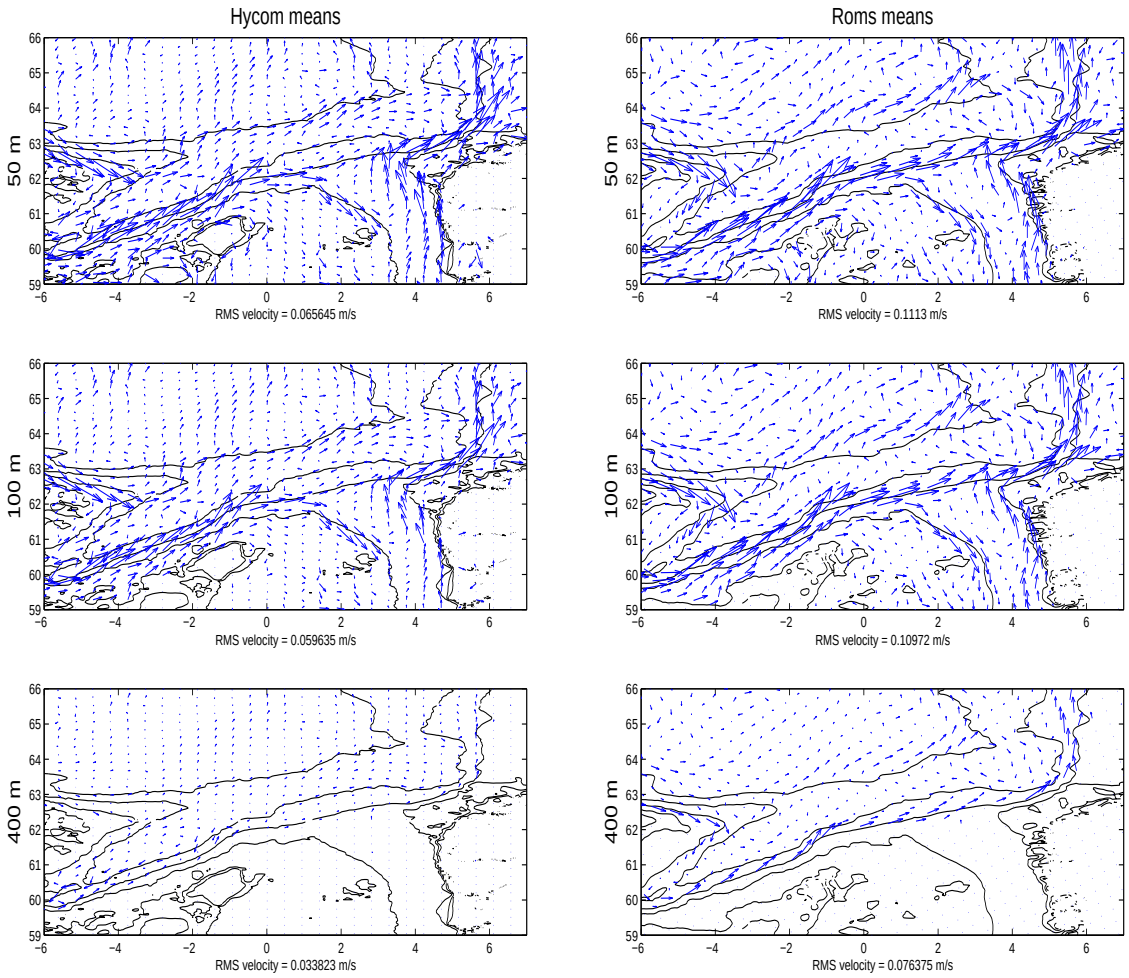

Figure 9: Velocity vectors from the HYCOM (left panels) and ROMS (right panels) simulations at 50, 100 and 400 m.

We also note that the fields of the two MIPOM simulations are nearly identical, implying the change in boundary condition has little impact on the mean velocities in this region (note the rms velocities are also nearly the same).

Figure 9 shows the similar HYCOM and ROMS mean vectors. The velocities in HYCOM are weaker, as seen in the left-hand panels. However there are a few additional points of interest. As in the MIPOM simulations, the inner branch mostly detours into the North Sea. But a small portion of the inner branch separates and continues along the 500 m isobath. We also see evidence of an outer branch. This was missed in the HYCOM speed contours in Figure 7 because the velocities are weak. The velocities at 400 m are also quite weak, and as with the MIPOM means, the flow near the shelfbreak is to the south, towards the North Atlantic. So HYCOM also exhibits a flow reversal with depth in the core of the inner branch.

The ROMS means are shown in the right-hand panels of Figure 9. The inner branch clearly bifurcates, with a majority proceeding along shelfbreak rather than flowing into the North

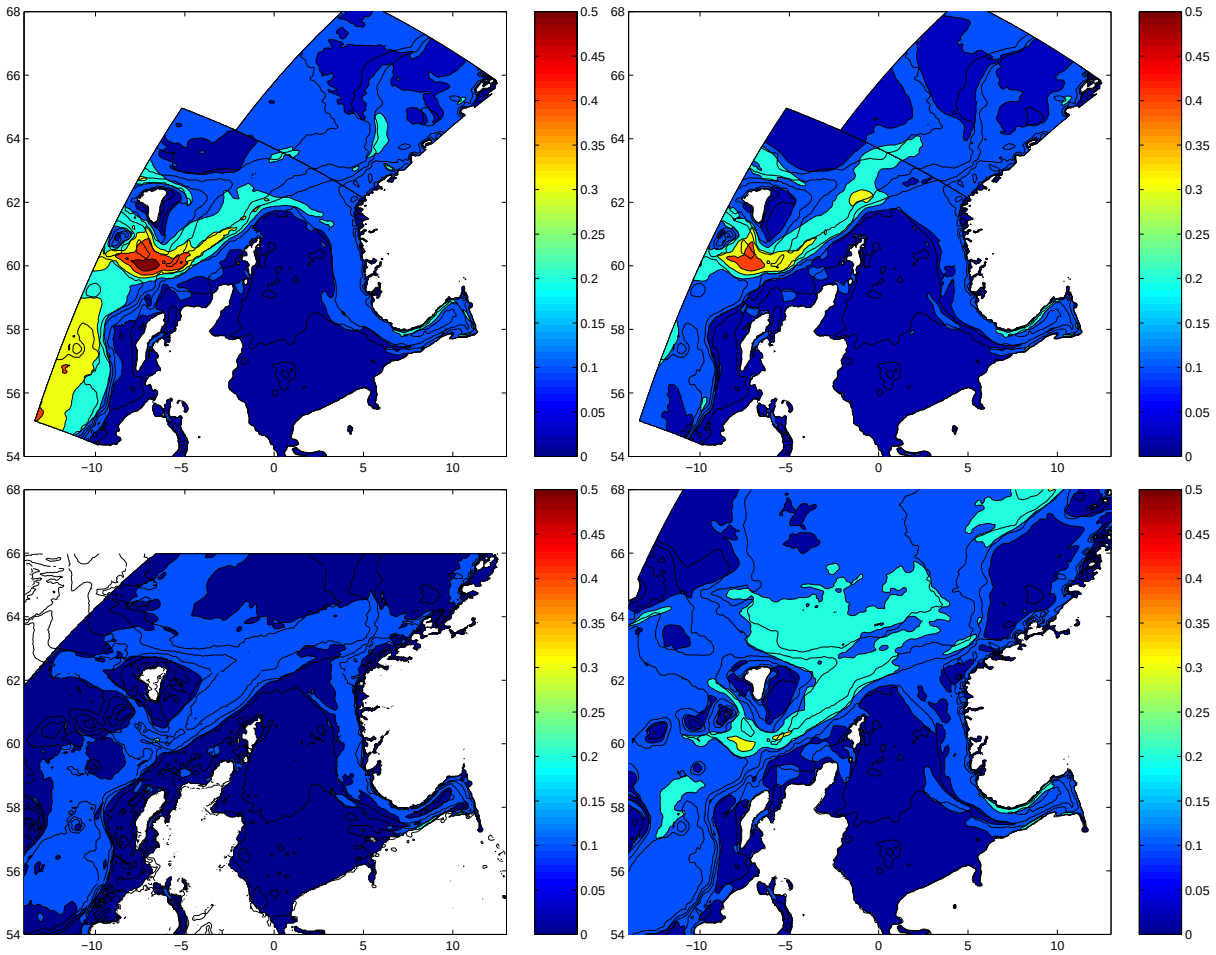

Figure 10: The standard deviation of the speed from the MIPOM/TOPAZ run (upper left panel), MIPOM/EKASC run (upper right panel), HYCOM run (lower left panel) and ROMS run (lower right panel), at 50 m depth.

Sea. Interestingly, the flow at 400 m is *also* poleward along the shelfbreak. So the ROMS simulation is the only one in which the inner branch doesn't reverse with depth.

4.3 Model standard deviations at 50 m

To assess the variability, we contour the standard deviation of the current speed. As with the means, we use the same geographical limits and color ranges for the models, to facilitate comparisons. We begin again with the large scale fields at 50 m depth, then look at the restricted domain at the three different depths.

4.3.1 50 m

Next consider the standard deviations of the speed as displayed in Figure 10. In general, the greatest variability occurs in the vicinity of the mean flows, suggesting the mean flows are

the principal source of variability in the model. Current instability is the most likely reason of this, although current meandering will also contribute to the standard deviation. The deviations are on the order of 10 cm/sec near the cores of the mean flow, except south and east of the Faroes where they are greater. The region just south of the Faroes in particular exhibits strong variability.

The MIPOM/TOPAZ simulation produces very similar standard deviations over much of the domain. However the deviations are somewhat greater in the southwest region of the domain. This may reflect stronger means in the TOPAZ boundary data, but it is also possible this may come from the small scale eddies present in the TOPAZ data. On the whole however, there are more similarities between the MIPOM/EKASC and MIPOM/TOPAZ runs than differences.

The HYCOM simulation produces deviations structurally like those in the MIPOM runs. But the HYCOM deviations are of order 10 cm/sec, whereas the MIPOM deviations exceed 20 and even 40 cm/sec. Interestingly, HYCOM does not exhibit the heightened variability to the west of Scotland, despite having TOPAZ boundary forcing. The reason for this difference with MIPOM/TOPAZ is not known.

The ROMS deviations are also qualitatively like those in the MIPOM runs, but the variability is greater, with the region with deviations exceeding 20 cm/sec covering a larger region. So while the variability near the outer branch in MIPOM is largely confined to the jet region, it spreads much further in ROMS. This is consistent with inferences from data, which suggest the outer branch is less stationary than the inner branch and that eddies are filling the region (*Poulain et al.*, 2001; *Orvik and Niller*, 2002; *LaCasce*, 2005). There is also greater variability to the north, near the Vøring plateau, than in the MIPOM simulations.

Note that in all the model runs, the maximum standard deviations are less than the maximum mean velocities. While the maximum means in the ROMS simulations are of order 50 cm/sec, the maximum standard deviations are roughly half that. This is probably unrealistic, as the eddies spawned from the mean flows should have similar maximum velocities as in the cores of the mean currents. So the models, at 4 km resolution, are probably still too dissipative to capture the full variability.

4.3.2 Vertical variation

Here we examine the vertical variation of the speed standard deviations (Figures 11 and 12). The change with depth is in general consistent with that seen with the mean velocities. Specifically, the deviations at 100 m are similar to those at 50 m, while those at 400 m are weaker.

The two MIPOM fields are very similar, indicating again that the change in boundary condition induces relatively small differences. However, there are some local changes, for example the greater variability north of Ormen Lange with TOPAZ boundary forcing.

Again the HYCOM fields are the weakest, throughout the water column. The ROMS deviations at 100 m depth are like those at 50 m, with the region with heightened variability extending offshore equally far at both depths. The deviations at 400 m are weaker, with the largest values occurring in the core of the inner branch, before the entrance to the North Sea.

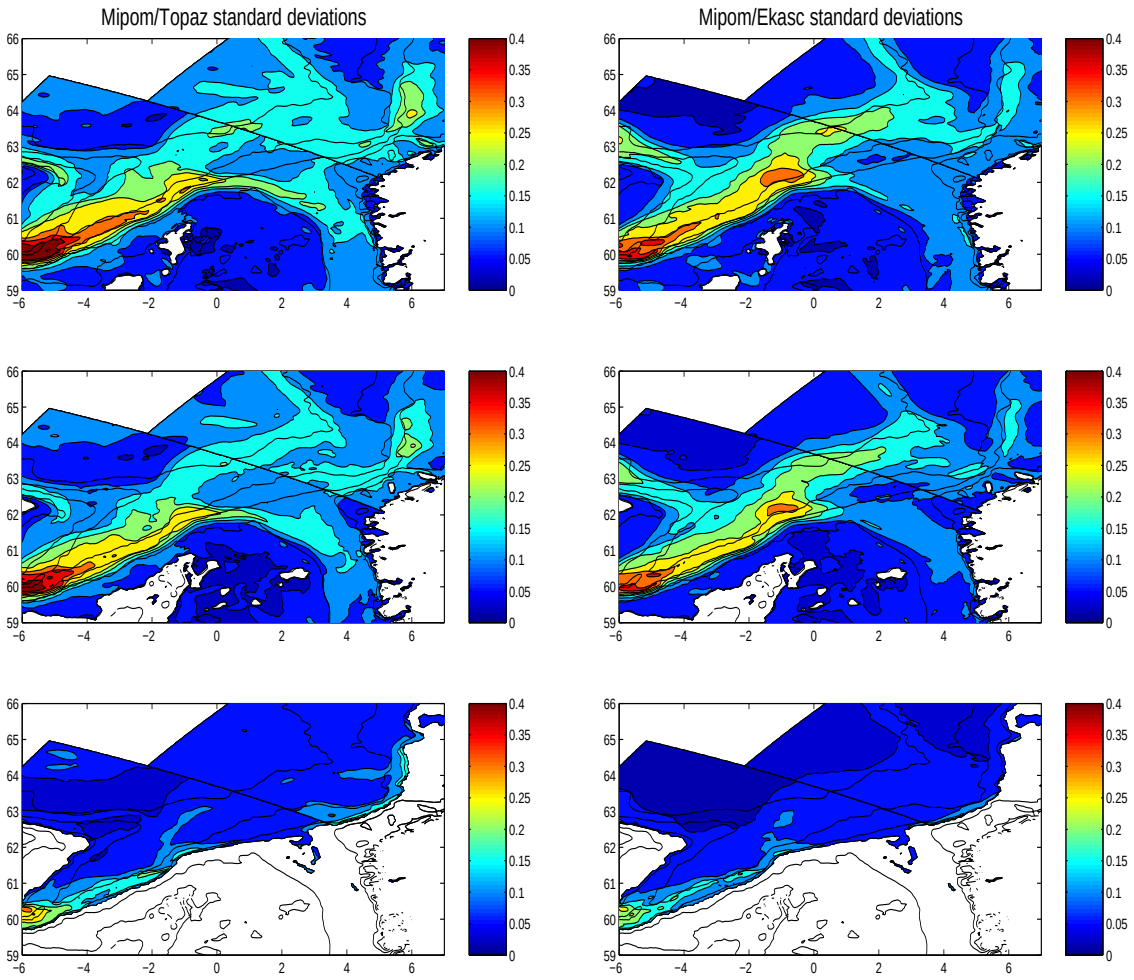

Figure 11: The standard deviation of the speed, at 50, 100 and 400 m, in the MIPOM/TOPAZ (left panels) and MIPOM/EKASC (right panels) simulation. The color scales are in m/s and range from 0 to 0.4 m/s.

4.4 Profiles

Now we focus in more detail at the response at one location. We choose Svinøy, because we have current meter data here spanning a period of several years (Figure 13). The data dates from the late 1990's and so does not overlap in time with the model simulations. But statistical comparisons are still possible, and are facilitated by the length of the records. The current meters are labeled S1 (nearest the shelfbreak, over the 500 m isobath), S2 (at mid-slope, near the 700 m isobath), Se1 (over the 900 m isobath) and Se2 (near the 1000 m isobath). We will begin at S1 and then work our way offshore.

Earlier analyzes suggest the inner branch is strongly steered by topography, including at Svinøy, e.g., *Mauritzen* (1996), *Poulain et al.* (2001), *Skagseth and Orvik* (2002) and *LaCasce* (2005). The observations also suggest the flow in the core of the inner branch is poleward, throughout the water column.

Hereafter, we use four statistics to compare the four models and the observations, as follows:

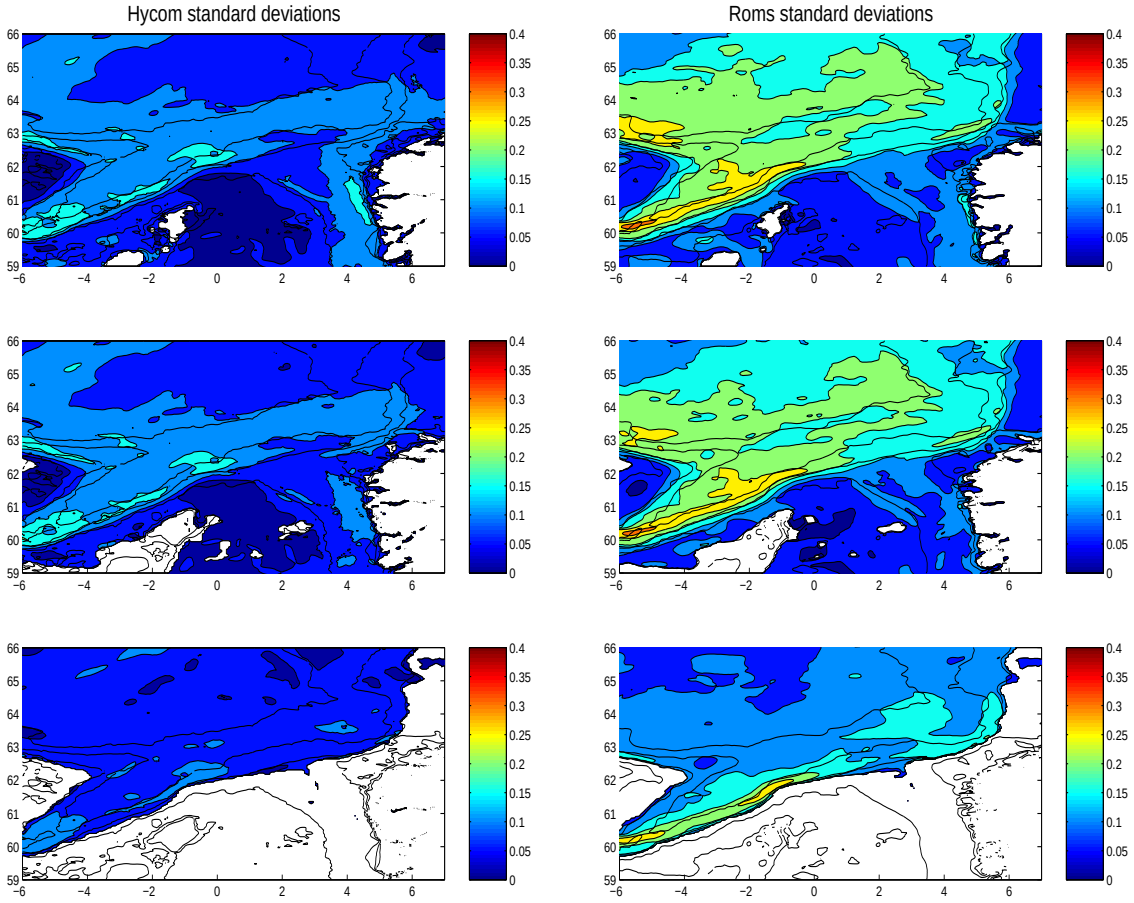

Figure 12: The standard deviation of the speed, at 50, 100 and 400 m, in the HYCOM (left panels) and ROMS (right panels) simulations. The color scales are in m/s and range from 0 to 0.4 m/s.

1. We calculate probability density functions (PDFs) of the current direction relative to the isobaths. To do this, we calculate the current direction from the daily mean velocities, and then calculate the angular deviation from the isobaths. An angle of 0° means flow parallel to the isobaths (poleward), while 180° means flow anti-parallel to the isobaths (equatorward). A positive angle implies upslope flow while a negative angle means downslope flow. We then bin the angles, making a histogram, and normalize it to obtain a PDF (the integral under the PDF should equal one). If the currents are strongly steered, the PDF should be sharply peaked around zero.

2. We then calculate PDFs of the current speeds. The speed is of course the magnitude of the daily current. These PDFs will show differences in the mean and standard deviation of the speeds, as well as in the frequency and amplitude of extreme currents. The speed PDF is also normalized, so that the integral of the curve is one. Because the speed is positive definite, the PDFs span only positive values. So they would necessarily be compared to a Rayleigh distribution rather than a Gaussian one.

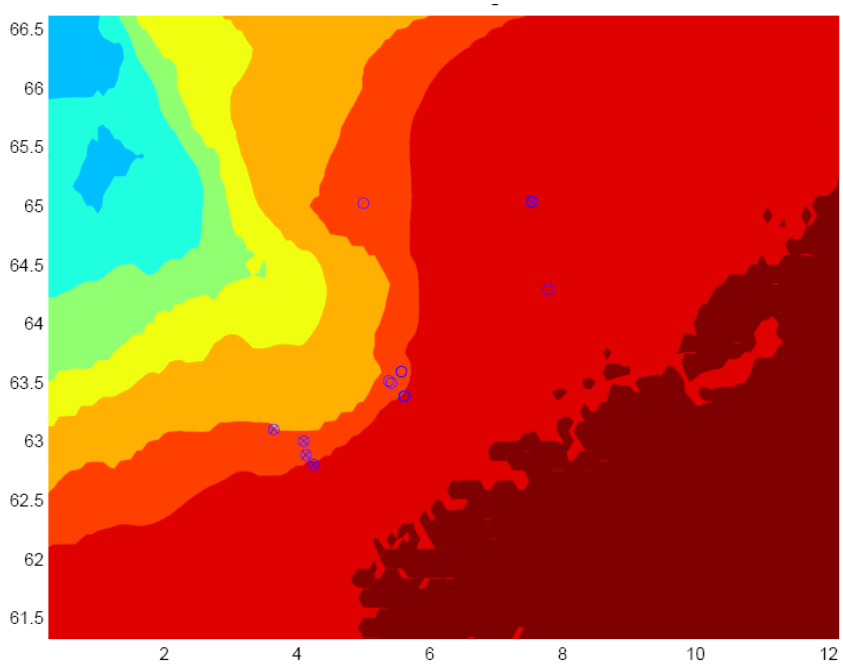

Figure 13: Map showing the locations of observations longer than one year (empty circles) and two years (x) in the Ormen Lange area. Colour scale shows topography with a contour interval of 500 m. Numbers along axes are longitude (horizontal axis) and latitude (vertical axis). The four locations in the lower left corner corresponds to the observations referred to as the Svinøy section.

3. We then examine the vertical shear in the mean currents, by averaging the along-isobath velocity at the different depths.

4. Then we plot the standard deviation of the speed as a function of depth.

4.4.1 S1

We begin near the shelf-break, in the core of the inner branch. A small problem with the data here is that the current record exhibits sudden, discontinuous changes in current direction, every year or so. We believe these occur due to changes in the mooring position, following servicing events of the instrument (*LaCasce*, 2005). The changes affect the current direction, but not, apparently, the magnitude. So we used a one year portion of the record to calculate the direction PDF, but the entire record for the speed PDF.

The direction PDFs for the four models are shown in Figure 14, with the PDF from the observations overlaid in red. At 100 m depth (upper four panels) the latter is sharply peaked, with the maximum near zero degrees. The peak actually lies at a positive angle, implying upslope flow. This may be real, but it may also stem from differences in the smoothed topography (derived from the etopo5 set plus local information as explained in *Engedahl et al.*, 1997, page 12) and the actual bottom. Most striking though is that the angle is nearly always

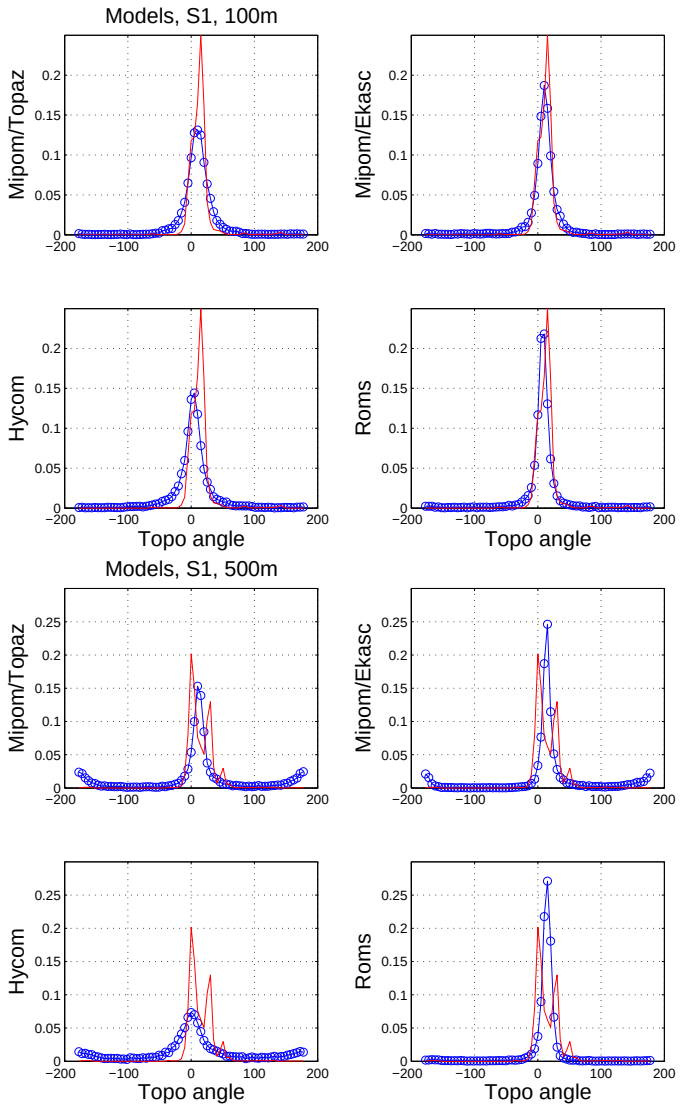

Figure 14: The direction PDFs at location S1. Upper four panels are near the surface at 100 m depth, while the lower four panels are near the bottom at 500 m. Note that the angle is relative to the isobaths so that zero points northword along the isobath, while ± 90 is onshore/offshore across the isobath, respectively. In this and the similar figures to follow the panels are ordered as in Figure 7.

between roughly -10 and +40 degrees; so the flow deviates little from the isobaths. Current meanders must be limited here, and eddies, if present, are not as strong as the mean.

The model PDFs at 100 m depth are very similar to the observed. The MIPOM/EKASC and ROMS runs exhibit tighter angular distributions than the other two, a difference perhaps due to the different boundary conditions. But otherwise the models are in reasonable agreement with observations.

The direction PDFs from the velocities at 500 m is shown in the lower four panels in Figure 14 (the in situ instrument is actually at 480 m depth). The PDF from observations is noisier than that at 100 m, and moreover exhibits multiple peaks. This is due in part to the shortness

of the record (one year) and from using too many bins when constructing the histogram (the peaks go away if the bin number is reduced). The PDF nevertheless indicates that the flow is restricted to a small range of angles, as at 100 m.

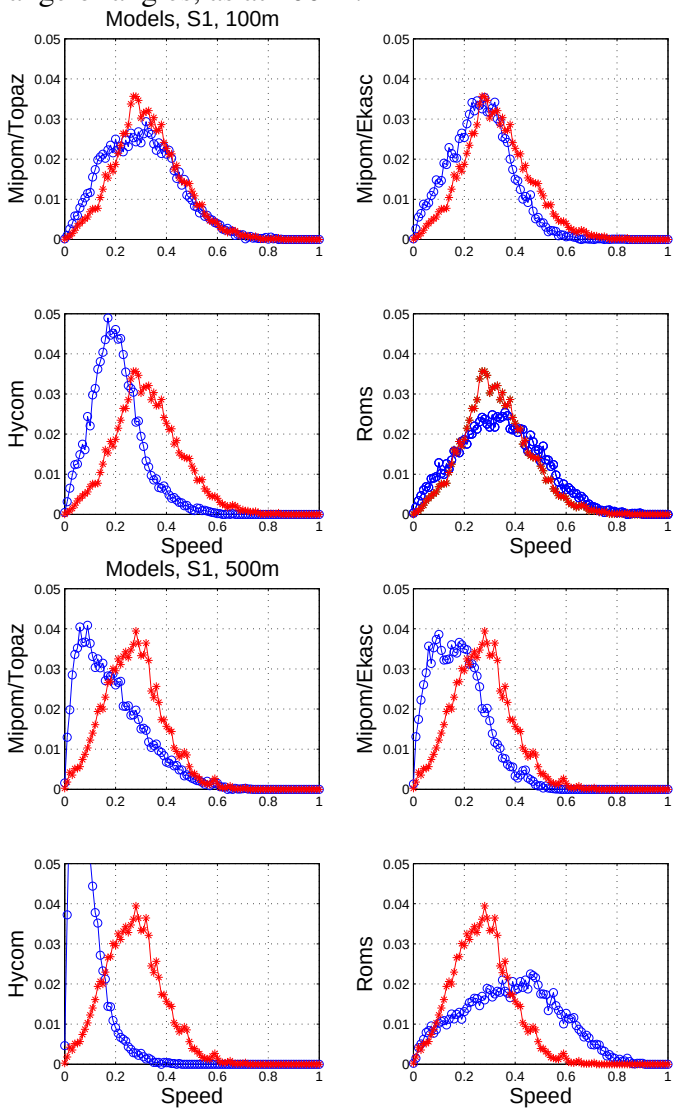

Figure 15: The speed PDFs at location S1 for the four models. Upper four panels are near the surface at 100 m depth, while the lower four panels are near the bottom at 500 m. Speeds along the horizontal axis are in m/s. Otherwise as in Figure 14.

As at 100 m, the ROMS and MIPOM/EKASC distributions are sharper than the HYCOM and MIPOM/TOPAZ distributions. But there are other points. All the PDFs except from ROMS have a small, secondary peak, centered near 180°. This implies that the flow is *reversing*. As the peak occurs in both the MIPOM/EKASC and MIPOM/TOPAZ distributions, it is not a consequence of the boundary conditions. Interestingly the reversals also occur in HYCOM, which uses a different vertical coordinate at depth (isopycnic, rather than terrain-following); so the reversals are not the result of the pressure gradient error which is known to affect sigma-coordinate models like MIPOM. Only the ROMS PDF exhibits little evidence of reversals.

The main peak in the HYCOM PDF is broader and weaker than in the other PDFs and this implies less severe topographic steering. Because the MIPOM/TOPAZ PDF has a narrower peak, this is not a consequence of the TOPAZ boundary conditions. It may stem instead from the choice of vertical coordinates. Indeed, remembering that HYCOM is a hybrid vertical coordinate, it has actually a much lower vertical resolution than the other two models at the S1 location (about 8 vertical active layers against 26 for MIPOM and 36 for ROMS).

The speed PDFs for the S1 instrument at 100 m are shown in the upper four panels of Figure 15. Consider for example the MIPOM/EKASC PDF, shown in the uppermost right panel. This resembles the observed PDF, but it is shifted to the left. This implies that the mean speed is lower in the model run. The PDF however has a width similar the observed, meaning the model standard deviation is not much different than from the data. Lastly, the model PDF goes to zero faster than the observed, so the model maximum velocities (the extrema) are weaker than observed.

The MIPOM/TOPAZ distribution is similar. However, it does a better job at capturing the large velocities. This means the TOPAZ boundary conditions yield more energetic currents at S1 than do the EKASC conditions. But the PDF is still shifted to the left compared to the observed PDF, so the mean velocity in MIPOM/TOPAZ is too low.

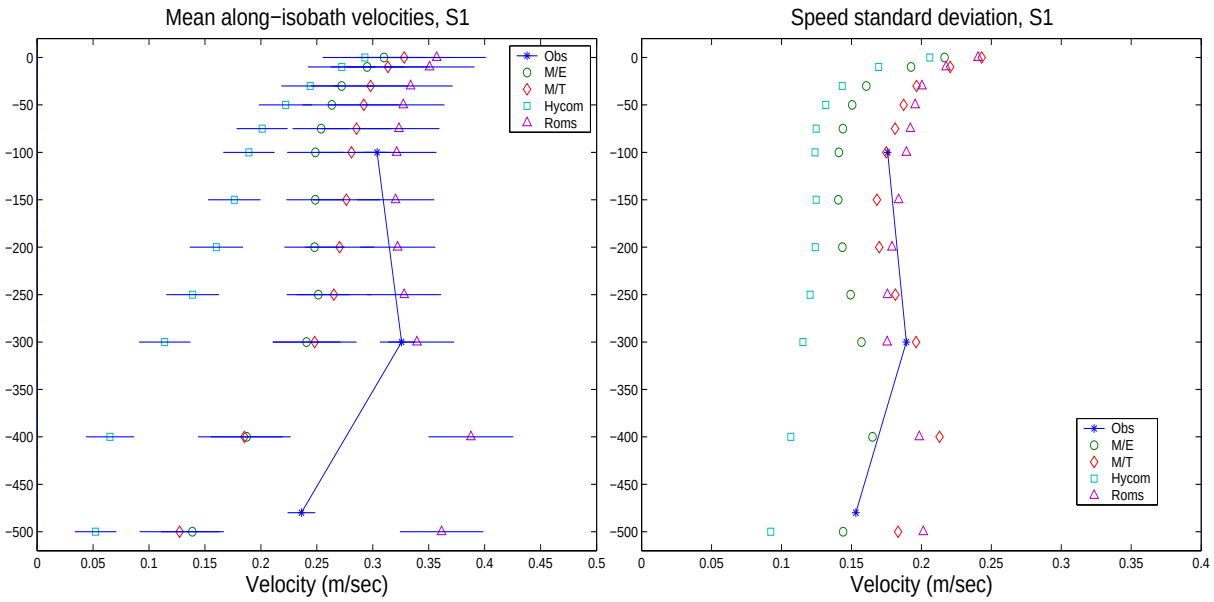

Figure 16: The mean along-isobath velocity (left panel) and standard deviation of the speed (right panel) at S1 as a function of depth, for the models and for the three in situ instruments. The error bars indicate the 95 % confidence intervals.

The ROMS PDF spans a similar range of current speeds as the data. However the ROMS PDF is actually somewhat broader than the observed, meaning the model standard deviation is actually too large. The HYCOM PDF on the other hand has consistently too weak velocities, and both the mean and standard deviation are too small. Note this is in spite of the fact that

the TOPAZ boundary conditions give larger maximum velocities in MIPOM.

The speed PDFs at 500 m depth at S1 are shown in the four lower panels of Figure 15. As at 100 m, the three models (MIPOM/TOPAZ, MIPOM/EKASC and HYCOM) are shifted to the left of the observations, indicating weaker means. ROMS on the other hand lies to the right, indicating a too strong mean.

We now tally the means and standard deviations as functions of depth (Figure 16). The observed mean is roughly 30 cm/sec and does not vary greatly with depth. It is still nearly 25 cm/sec near the bottom. Of the models, ROMS produces the strongest mean flow, followed by the MIPOM/TOPAZ, MIPOM/EKASC and HYCOM models. The ROMS means are moreover not different from the observations at the 95 % confidence level, except at the deepest level where they are too strong. Note too that the two MIPOM means are not significantly different; so the change in boundary conditions does not alter the mean at S1 in MIPOM. The HYCOM mean is significantly weaker than all the others.

The observed standard deviations (Figure 16 right panel) are between 15-20 cm/sec. The model deviations are similar, with ROMS producing the most energetic variations and HYCOM the least ones. MIPOM/TOPAZ and MIPOM/EKASC are in between with MIPOM/TOPAZ more energetic than MIPOM/EKASC. ROMS is in line with the observations, except near the bottom where it is again slightly too energetic. Interestingly, the MIPOM/TOPAZ deviations are also slightly too strong at depth, and the MIPOM/EKASC simulation exhibits bottom-intensified variability as well. It is possible this bottom-intensification is a sign of topographic waves. Only HYCOM shows no evidence of this effect.

Note too that all the models exhibit significantly larger deviations in the upper 20 m, implying large shears in the surface layer. This was noted as well by *LaCasce and Engedahl* (2005) with regards to an earlier MIPOM simulation. This shear cannot be checked with these observations.

4.4.2 S2

Now we proceed to S2, over the mid-slope. Unlike with S1, there are no abrupt changes in current direction with S2; so we can use the entire (approximately 3 year) records for the direction PDF.

The direction PDF (Figure 17) from the observations is like that at S1, centered nearly at zero degrees and exhibiting a fairly small range of angles. The model PDFs are similar to the observed, particularly the ROMS and HYCOM PDFs which have nearly the same narrow central peak. The MIPOM PDFs exhibit a larger range of angles. They are moreover similar, indicating little effect from the change in boundary conditions. There is some evidence of flow reversal in the ROMS simulation; this is not seen in the other models nor in the observations.

At 700 m (Figure 17 lower four panels), the direction PDF from the observations exhibits a primary peak near zero and a secondary peak at 180°. The latter again indicates flow reversals. But as this peak is much smaller than the one at 0°, we conclude the flow is most often poleward.

The ROMS PDF is quite similar to the observed. The central peak has the same height, and there is a lesser secondary peak at 180°. The latter is somewhat larger than observed, but the flow here is still most often poleward. In the other three cases (MIPOM/EKASC,

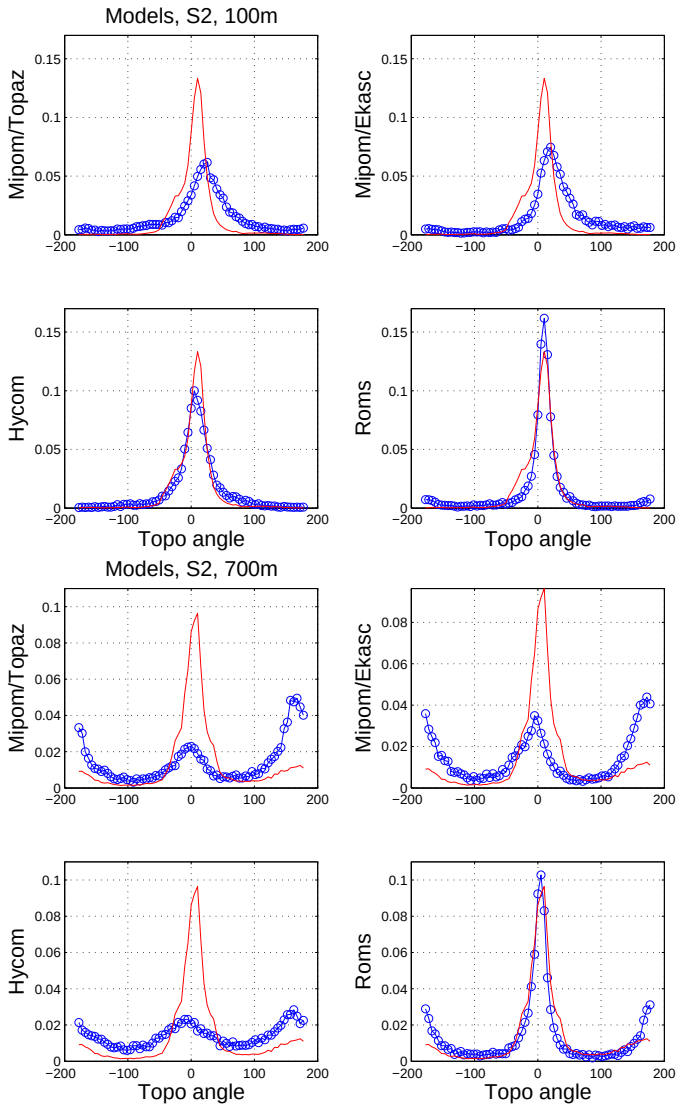

Figure 17: The direction PDFs at location S2. Upper four panels are near the surface at 100 m depth, while the lower four panels are near the bottom at 700 m. Otherwise as in Figure 14.

MIPOM/TOPAZ, HYCOM), the reversals are more frequent and the central peak is diminished. So the flow in these models is as often equatorward as it is poleward. Note the MIPOM/TOPAZ central peak is smaller than that of MIPOM/EKASC, but this is a relatively minor difference.

Regarding the speed PDFs at 100 m at S2 (Figure 18 upper four panels) the PDF from the observed velocities closely resembles that at S1. The model PDFs indicate weaker means and standard deviations than observed, although the ROMS PDF comes closest to the observations (and has a similar high-velocity tail).

Moreover, the speed PDFs at 700 m (Figure 18 lower four panels) show that HYCOM, MIPOM/TOPAZ and MIPOM/EKASC exhibit too weak means and deviations, although the MIPOM/TOPAZ PDF is not far off. ROMS again has a PDF which is closest to the observed, although the model again overestimates the standard deviation and the maximum velocities (note difference in scaling which enhances this overestimation compared to the other models).

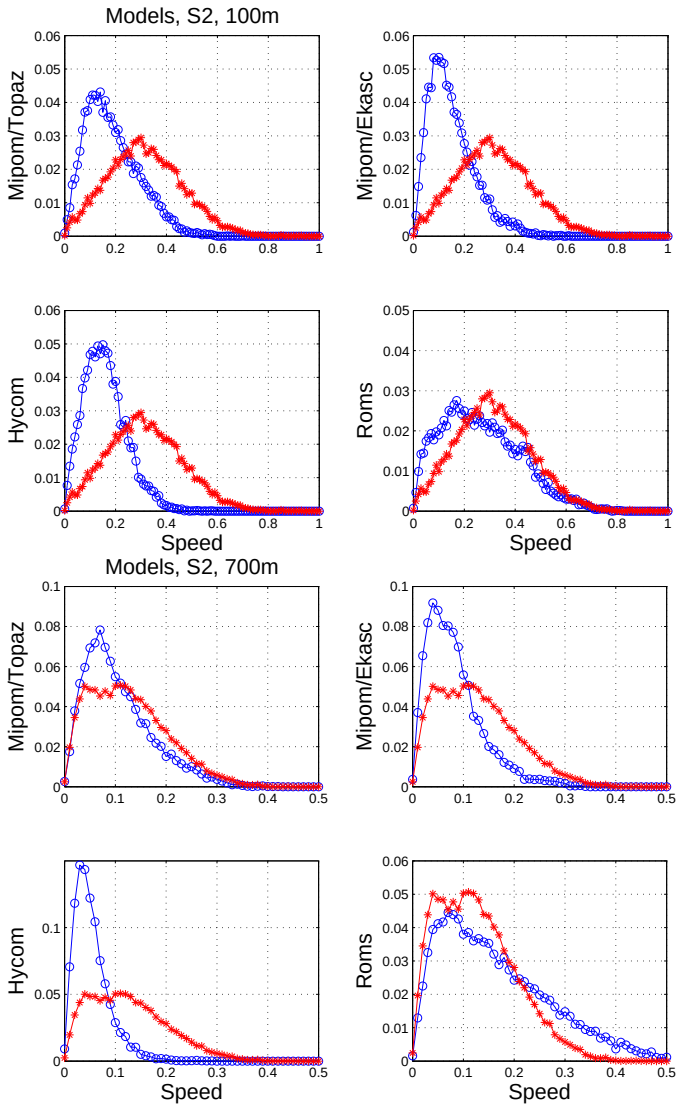

Figure 18: The speed PDFs at location S2. Upper four panels are near the surface at 100 m depth, while the lower four panels are near the bottom at 700 m. Note difference in vertical scaling among the models. Otherwise as in Figure 15

The cumulative effect of the PDFs is seen in the means and standard deviations (Figure 19). The observed mean is strongly sheared but is still clearly poleward, even at the deepest instrument. The same is true with the ROMS mean, which is comparable to the observed mean at depth although somewhat weaker above 300 m. The other three models exhibit means with approximately the correct shear, but the depth-averaged velocity is too weak, causing the means to cross zero, typically at around 400 m.

The observed standard deviations decrease with depth, from 20 cm/sec at 100 m to about 12 cm/sec at 700 m. The MIPOM/TOPAZ run has very similar deviations. ROMS exhibits too energetic variability, as at S1, while the other two models are weaker. Again the models exhibit heightened variability in the upper 20 m or so, particularly HYCOM and MIPOM/EKASC.

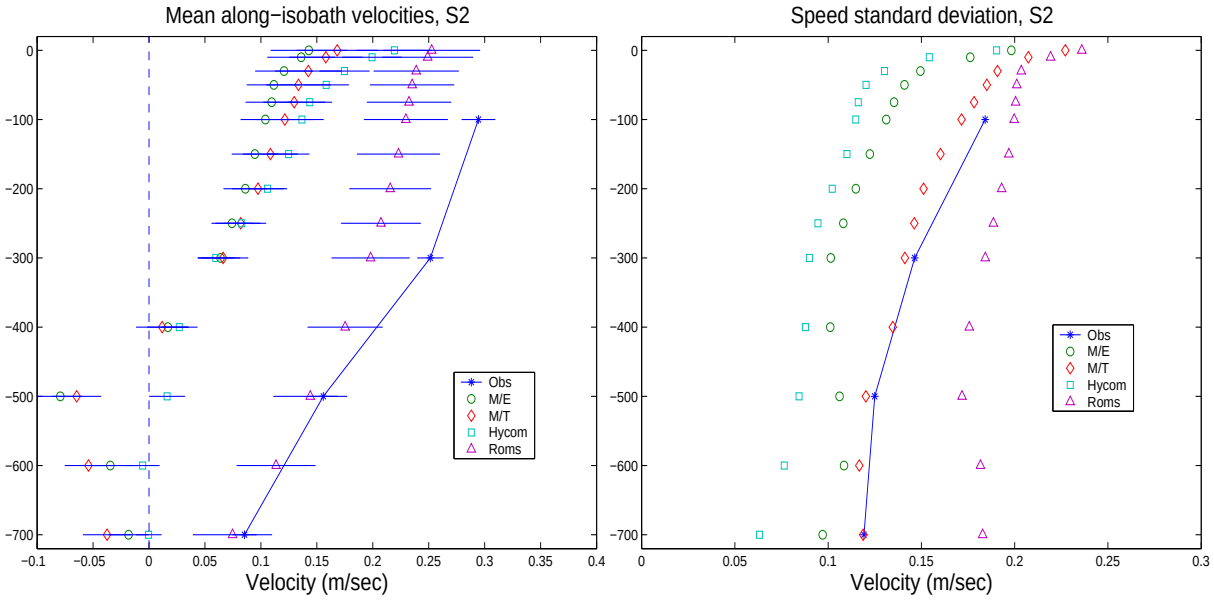

Figure 19: As Figure 16 except at S2.

4.4.3 Se1

As noted, mooring Se1 lies further out on the slope, near the 900 m isobath. The direction PDF from the observations (Figure 20) exhibits a peak, near 20°, indicating upslope flow. However, we see too that there is an increased likelihood that the flow will be essentially in any direction, as the probability is around 0.01 over a range of angles. We infer that eddy activity is more pronounced here.

The model PDFs likewise exhibit higher probabilities for flow in any direction. The two MIPOM simulations show little preference for a single direction, except the MIPOM/TOPAZ simulation which shows higher probability around 50 ° and the MIPOM/EKASC simulation which shows greater likelihood for upslope than downslope flow. The HYCOM simulation produces a peak near the observed peak, near 20°, but somewhat more diffuse than in the observations. This indicates a possible advantage of using isopycnic coordinates in open deeper waters. ROMS shows a clear peak near 20°, even sharper than in the observations. This means there is somewhat less variability in flow direction in ROMS than observed.

The PDF for the near-bottom flow at Se1, at 900 m depth (Figure 20 lower four panels) is similar to that at 100 m; there is a peak, centered around 10-20° and a uniform background distribution with probabilities of around 0.01. The peak is flatter than at 100 m, indicating equal probabilities in the range -20° to 30°.

The models again exhibit southward flow, towards the North Atlantic, but the extent to which this is true varies. The MIPOM simulations have almost no central peak, indicating the flow is rarely poleward. HYCOM exhibits a small central peak so the flow is occasionally poleward; however it is more often equatorward, and hence the mean will also be southward. ROMS exhibits some southward flow, but the central peak is larger implying the flow is pri-

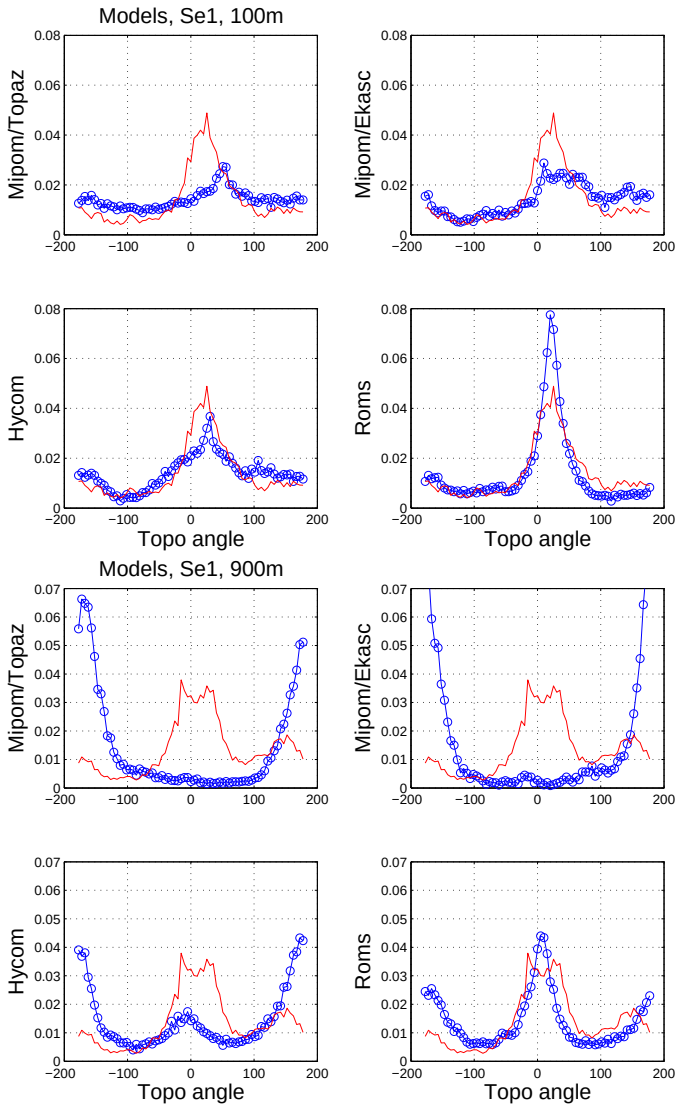

Figure 20: The direction PDFs at location Se1. Upper four panels are near the surface at 100 m depth, while the lower four panels are near the bottom at 900 m. Otherwise as in Figure 14.

marily poleward. So of the four models, ROMS is the most often correct here.

The speed PDFs at Se1, at 100 m depth, are shown in Figure 21 (upper four panels). The ROMS PDF is not significantly different from the observed. The other three models again have weaker means and standard deviations. At 900 m (Figure 21 lower four panels), ROMS again produces a PDF which is remarkably similar to the observed. The MIPOM/EKASC and MIPOM/TOPAZ PDFs on the other hand are both indicative of too weak means. Furthermore, as inferred from the direction PDFs, these means are pointed in the wrong direction. HYCOM exhibits the weakest mean of the group with velocities which are typically less than 15 cm/sec.

The plot of the mean velocities as functions of depth (Figure 22 left panel) supports these inferences. The ROMS means are identical to the observed, within the error bars. HYCOM produces a weak northward flow about 300 m and a weak southward flow below 400 m. The two MIPOM means differ the most from observations, having a strong southward flow below

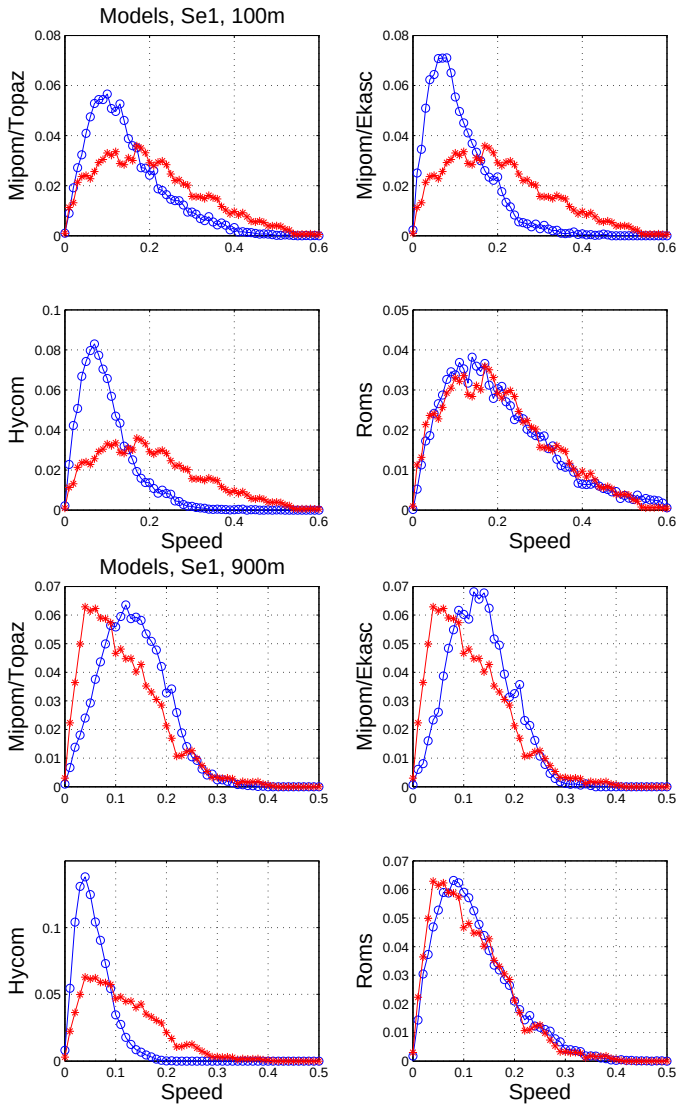

Figure 21: The speed PDFs at location Se1. Upper four panels are near the surface at 100 m depth, while the lower four panels are near the bottom at 900 m. Note difference in vertical scale applied to ROMS at 100 m depth and HYCOM at 900 m depth. Otherwise as in Figure 15

300 m. Unlike at S2, this cannot be written off as having a too-weak depth-averaged flow, because the vertical shear here is also much greater than observed.

Regarding the standard deviations (Figure 22 right panel) ROMS produces the correct deviations at the deepest and shallowest instruments, but slightly too large deviations at mid-depths. The other models produce too weak deviations over the range of depths, with MIPOM/TOPAZ being relatively the strongest and HYCOM the weakest. Again, the models exhibit strong shear in the surface layers, particularly HYCOM and MIPOM/EKASC.

4.4.4 Se2

Lastly we examine mooring Se2, near the 1000 m isobath. This lies essentially out of the inflow, so the observed direction PDF at 100 m (Figure 23 upper four panels) does not exhibit

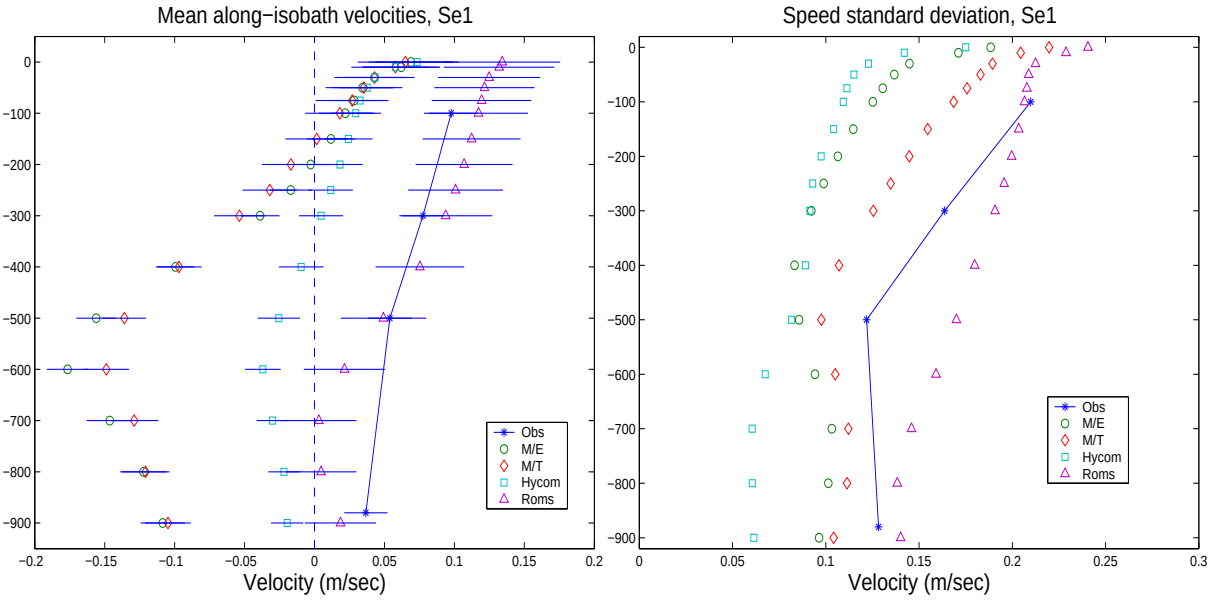

Figure 22: As Figure 16 except at Se1.

a clear peak near 0°. Rather, the PDF ranges between 0.01 and 0.02 over the full range of angles, with an indication of a greater likelihood for onshore than offshore flow.

The ROMS directional PDF is remarkably similar, nearly tracing out the observed PDF (so the model could probably be used to deduce the reason for the onshore flow). HYCOM too yields a very similar PDF. The MIPOM simulations on the other hand insist on southward flow. So while this flow was only evident at depth at S2 and Se1 in MIPOM, it is also present at 100 m at Se2.

The direction PDFs at the level of the deepest instrument (900 m; Figure 23 lower four panels) paint a similar picture. ROMS and HYCOM have PDFs very close to the observed, while MIPOM has a distinctly equatorward tendency. In fact, the ROMS and HYCOM directional PDFs are remarkably similar. In this instance , ROMS and HYCOM tends to give complementary informations and both could be used to explain the onshore currents at 100 m and offshore currents at 900 m.

The speed PDFs for the 100 m level are shown in Figure 24. In this case, ROMS and MIPOM/TOPAZ produce nearly perfect distributions. The mean in the MIPOM/EKASC PDF is on the other hand too weak, and that in HYCOM even weaker. So TOPAZ forcing produces a better distribution in MIPOM, but not in HYCOM. Recall though that the MIPOM velocities have a false southward tendency.

The speed PDFs for the 900 m level are shown in Figure 24 (lower four panels). In this case, ROMS is closest to the observed distribution, albeit with a slightly larger mean. HYCOM again has a mean speed which is too weak. In both MIPOM simulations, the mean speed is too large.

We see the mean along-isobath velocity in Figure 25. We remind the reader that the mean along-isobath velocity, which can of course be zero, will differ from the mean speed if the

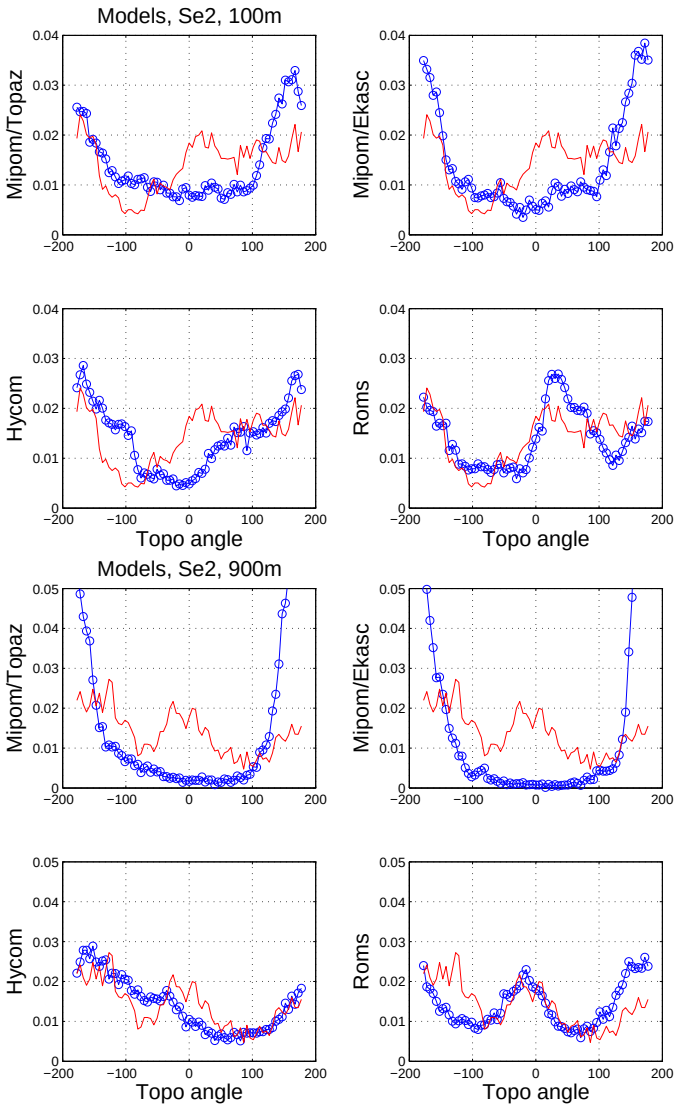

Figure 23: The direction PDFs at location Se2. Upper four panels are near the surface at 100 m depth, while the lower four panels are near the bottom at 900 m. Otherwise as in Figure 14.

current assumes a range of directions. The ROMS mean is in fact not different from zero at the 95 % level. The observed velocity however is weakly southward, at all depths. HYCOM also produces a weak southward flow, except near the surface. The two MIPOM simulations on the other hand have a southward flow which is intensified at about 500-600 m depth and has maximum velocities of 15 cm/sec.

The observed standard deviations (Figure 25 lower panel) approach 17 cm/sec above 500 m, and fall to 12 cm/sec below. MIPOM/TOPAZ and ROMS produce similar deviations, albeit slightly too weak and too strong, respectively. MIPOM/EKASC follows and HYCOM produces the weakest variability.

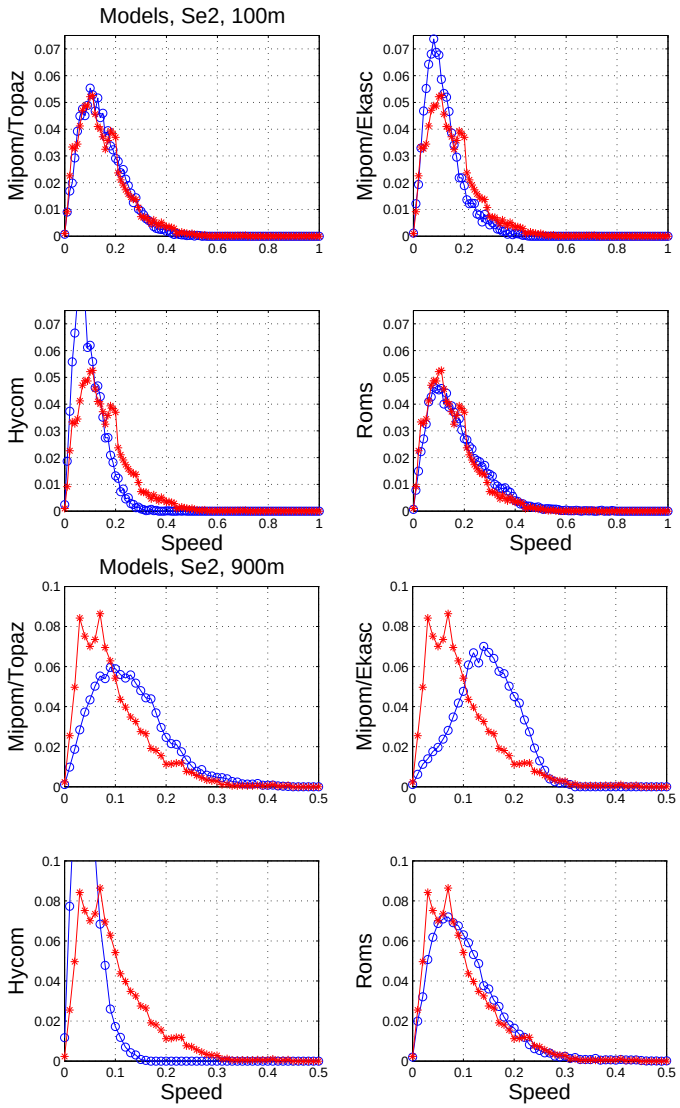

Figure 24: The speed PDFs at location Se2. Upper four panels are near the surface at 100 m depth, while the lower four panels are near the bottom at 500 m. Otherwise as in Figure 15.

4.5 Analysis summary

We have compared the response the four model simulations with various observations. We examined the two dimensional velocity fields at various depths as well as velocity statistics at the Svinøy site. The models produce similar large scale mean velocity fields, which moreover resemble our best estimates of the actual surface flow. All the models have an inflow from the North Atlantic in two branches, and these generally proceed poleward. There are small differences in the strengths and paths of the currents, but it is not possible at this point to say which is more realistic.

However, the models differ in a few important respects. All, or nearly all, of the inner branch in three of the models (MIPOM/TOPAZ, MIPOM/EKASC and HYCOM) detours into the North Sea rather than tracking the 500 m isobath poleward, off Norway. This suggests the current is too shallow in those models, following the 200 m isobath instead. ROMS on

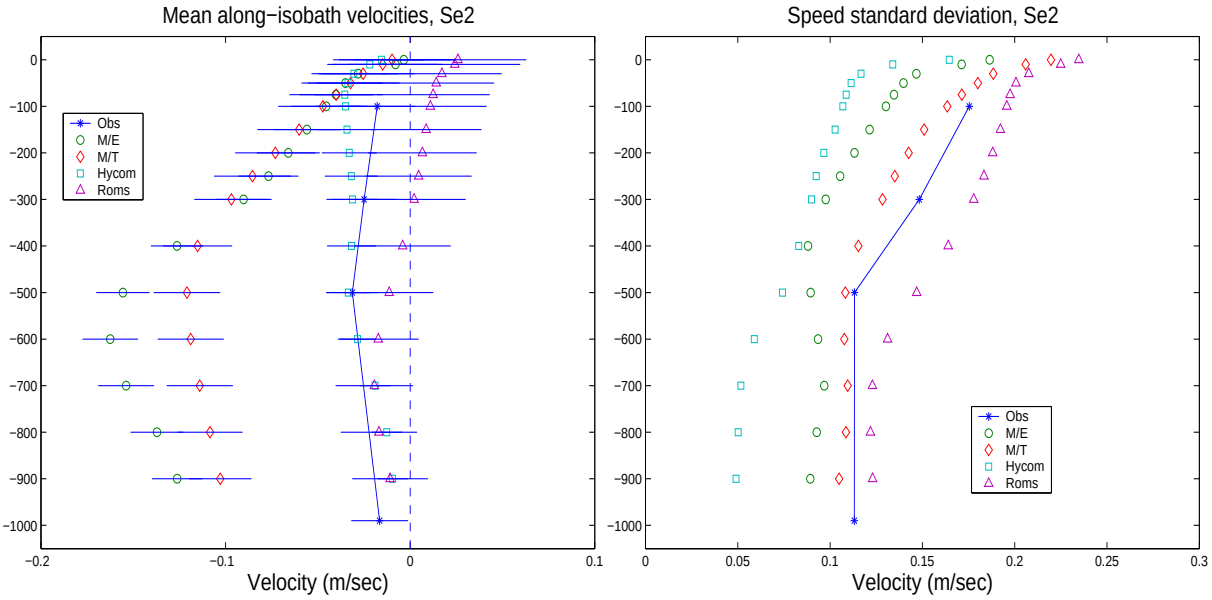

Figure 25: As Figure 16 except at Se2.

the other hand get this path mostly correct, as only a fraction peels off into the North Sea. Furthermore, the two MIPOM simulations produce a strong equatorward mean flow at depth, below and offshore of the inner branch. This is also seen to a lesser extent in HYCOM. ROMS on the other hand exhibits poleward flow over the entire water column. On the whole, HYCOM exhibits significantly weaker mean flows than the others.

The analysis of the Svinøy velocities supports these conclusions. ROMS is consistently the closest to the observations, both in terms of the direction and speed of the currents. ROMS is however too energetic in some locations, particularly at depth. HYCOM exhibits the weakest variability, but it should be noted that it is generally more successful at predicting current direction than MIPOM, particularly at the deeper locations. MIPOM has larger deviations than HYCOM and less than ROMS; its primary shortcoming at Svinøy is its equatorward flow, which dominates the current fluctuations, particularly outside of the core of the inner branch.

We conclude that ROMS is the most successful at capturing the various aspects of the observations. It would however be useful to understand why it overpredicts the deviations in certain instances.

5 Discussion

The main model differences which emerge from this analysis are 1) the paths of inner branch of the Atlantic inflow, 2) the existence of a southward mean flow under and adjacent to the inner branch and 3) the energetics of the various model flows. Let us consider each point in turn.

The difference in paths reflects that the core of the inner branch is at different depths in

the models. In MIPOM and HYCOM, the core is too shallow and thus a majority of the inflow tracks the 200 m isobath into the North Sea, and particularly so in MIPOM. HYCOM does show some additional flow along the 500 m isobath, but the majority is clearly shallower. The ROMS inflow on the other hand is primarily along the 500 m isobath, with less transport at shallower depths. One is tempted to conclude that the difference is a result of having terrain-following coordinates in ROMS, because this could produce superior topographic steering. But MIPOM also has terrain-following coordinates and does not produce as satisfactorily results. So if this is so, ROMS has a better implementation. In addition, HYCOM has isopycnic or z-coordinates, but behaves nevertheless very much like MIPOM. Another possibility is that ROMS uses more vertical levels than the other two models (see Table 1). But with water depths of 500 m and less, one imagines that MIPOM probably has sufficient vertical resolution. As discussed below, we believe a likely reason for the model difference on this point relates to the sophistication of the numerical methods used to handle horizontal and vertical advection in the model.

Similar comments apply to the second point. One would be tempted to ascribe the southward mean flow in MIPOM to the so-called pressure-gradient error, which is known to degrade terrain-following coordinate model performance near steep slopes. But the fact that HYCOM also exhibits the southward flow, without terrain-following coordinates, and that ROMS does not, with terrain-following coordinates (see however *Shchepetkin and McWilliams*, 2003), throws this explanation into doubt. One might also look towards the boundary conditions, because having an incorrect barotropic inflow could make the inner branch too baroclinic. But MIPOM displayed essentially the same southward flow with both TOPAZ and EKASC conditions. So the cause of this effect remains obscure.

The rationale behind the third problem is probably clearer. ROMS exhibits both stronger mean flows and more energetic variability. ROMS is also the only model which employs third-order advective schemes horizontally and a parabolic spline-based representation for the vertical advection. These are shown in previous studies to produce more realistically energetic flows (*Shchepetkin and McWilliams*, 2005; *Winther et al.*, 2007). Indeed, shifting from a second-order to a third-order scheme is effectively like increasing the model resolution. In fact, in recent experiments with MIPOM with 1.5 km resolution (not shown), we find that the inner branch successfully tracks the 500 m isobath, as in ROMS. This implies that ROMS, with 4 km resolution, is behaving like MIPOM with 1.5 km resolution. As the dominant eddy scale in this region is comparable to the deformation radius (roughly 10 km), having a higher-order advective scheme is likely critical. However, we note that MIPOM and HYCOM both used second order advection schemes, and MIPOM exhibited consistently more energetic fields. So the advection scheme is not the only determining factor.

The disadvantage of employing more sophisticated numerical methods is an increase in computer time. In fact ROMS uses a factor of two to three longer than MIPOM for a given simulation period. However, increasing the resolution by decreasing the grid size, which is another natural possibility, increases the computer time by a factor of about eight. Thus it is worthwhile to employ better numerics than just increasing the resolution to obtain better velocity distributions, particularly for the higher velocities.

It is interesting however that ROMS actually overestimates the eddy variability in some locations, notably at the lower depths over the slope. The reason for this is not known, nor is it known whether these velocities would be even more energetic at higher resolution. How-

ever, ROMS was run in these simulations without explicit lateral dissipation; only the implicit (equivalent fourth-order) dissipation associated with the advective scheme was acting to damp the motion. But one could easily include explicit damping and this would reduce the variability at depth. This would best be done in conjunction with data, to tune the strength of the damping to match the observed variability.

6 Summary and conclusions

We consider the results from a three year simulation employing three eddy-permitting numerical ocean models for a region along Western Norway (Figure 1). Two of them, MIPOM and ROMS, are terrain-following coordinate ocean models, while the third, HYCOM, is a hybrid coordinate model employing geopotential depth coordinates near the surface and isopycnic coordinates at depth.

The particular aim of the study is to assess whether ROMS or HYCOM can replace MIPOM for numerical ocean weather prediction in Norwegian waters. Ocean weather is connected to eddies, jets and meanders with a typical length scale of order 10 km in these waters (*Røed*, 1996; *Røed and Fossum*, 2004; *Fossum and Røed*, 2006; *Fossum*, 2006). It should be emphasized that these features are responsible for most of the high current events in the ocean.

All models employ approximately the same grid size ($\approx$ 4 km), and care is exercised in making the forcing (e.g., atmospheric input, river discharges, topography, initial conditions, lateral open boundary forcing, etc.) as similar as possible. Differences are nevertheless unavoidable. For one, ROMS and HYCOM were run with different lateral boundary forcings, referred to as EKASC and TOPAZ, respectively, while MIPOM was run with both. As such, the MIPOM/TOPAZ and HYCOM simulations are directly comparable as are the MIPOM/EKASC and ROMS simulations, but some care is required in comparing the ROMS and HYCOM simulations.

We focus on horizontal velocities for comparison with in situ measurements at the Svinøy section. As the observations generally do not overlap in time with the model simulations, and that the year to year variability in the currents may be significant, we focus on *statistical* comparisons of ling time series. This is also sensible in light of the active, small scale eddy field (*LaCasce and Engedahl*, 2005). In addition we have examined the spatial structure of the velocity means and standard deviations, at different depths.

The model mean flows and standard deviations are broadly similar in structure. However, there are differences in magnitudes, with ROMS usually more energetic in both measures than MIPOM, and MIPOM more energetic in turn than HYCOM. In addition, MIPOM exhibits an equatorward mean flow beneath the poleward warm inflow from the North Atlantic. HYCOM exhibits a similar flow, but much weaker. ROMS is the only model which exhibits a poleward mean flow at all depths in the inflow. Furthermore, the ROMS inflow bifurcates with the majority of the flow proceeding along the shelf break and a smaller portion floing into the North Sea. Also HYCOM bifurcates, but with the majority of the inflow flowing into the North Sea. In contrast the mean flow in MIPOM basically entirely flows into the North Sea, mixing with the Norwegian Coastal Current and thereby altering the water mass characteristics. The observations suggest this is not happening in reality and that the ROMS bifurcation is the most

realistic one.

The results at Svinøy indicate that the MIPOM and HYCOM fields are consistently too weak compared to the observations, while the ROMS velocities are closer to observed. In fact, the ROMS velocities are actually too energetic in certain locations. Curiously MIPOM velocities are consistently equatorward at depth, as opposed to the ROMS and observed velocities which are nearly always poleward. Overall the directions are better respected by HYCOM than by MIPOM, in particular at the deeper locations, but also HYCOM shows a higher tendency for equatorward flows at depth than indicated by the observations.

The success of the ROMS model in simulating the observed fields derives in part from its use of the third order horizontal advection scheme combined with a better vertical resolution and a more sophisticated numerical handling of the vertical processes. Use of the higher order advection scheme makes ROMS effectively less viscid, implying its effective resolution is higher than MIPOM and HYCOM for the given grid size. The result is an increase in the eddy activity. Thus the likelyhood of capturing more high current events increases. This conclusion is underscored by, e.g., *Winther et al.* (2007) who reported that replacing the second order scheme in HYCOM with higher order advective schemes resulted in higher eddy activity at the same grid resolution. In addition, higher order schemes are better at preserving small scale eddies, which in turn are so important for high velocity events. This is likely why the higher end of the velocity distributions are better captured by ROMS than the other models.

Using higher vertical resolution implies that ROMS has a better representation of the bottom topography. In addition its more sophisticated handling of the vertical processes produces more realistic upslope velocities. Taken together this may explain why ROMS is the only model giving a consistent poleward flow towards Svinøy at all depths.

The use of more sophisticated numerical methods and a higher vertical resolution however has a price. It increases the computer time by a factor of two to three. Optionally to increase the eddy activity, and thereby the eddy kinetic energy in HYCOM and MIPOM, the grid size could be decreased to say 2 km. However, the cost then is to increase the computer time by a factor of eight. Thus we find that use of sophisticated numerical methods is a far better option than increasing the horizontal resolution. Based on these results, we therefore recommend using ROMS as the main operational model for ocean weather predictions at **met.no** to replace MIPOM.

Acknowledgment

This research was supported in parts by a consortium of offshore industry companies named the Norwegian Deep-water Programme (NDP) and in parts by the participating institutions, namely the Norwegian Meteorological Institute (coordinator), Institute of Marine Research and the Nansen Environmental and Remote Sensing Center/Mohn Sverdrup Center. The NDP consortium consists of Conoco-Phillips, ExxonMobil, BP Norge, Norsk Hydro, Norske Shell, Statoil, Total and RWD Dea. The computations were performed at the Norwegian Supercomputer facilities.

References

Ådlandsvik, B., and W. P. Budgell (2003), Adapting the regional ocean model system for dynamic downscaling, in *RegClim General Technical Report*, vol. 7, edited by T. Iversen and M. Lystad, pp. 49–57, Norwegian Meteorological Institute.

Albretsen, J. (2007), Impact of freshwater effluence on the circulation in the Skagerrak/northern North Sea Part II: Energy analysis, *Revised version submitted to Ocean Dynamics March 27, 2007*.

Bleck, R. (2002), An oceanic general circulation model framed in hybrid isopycnic-cartesian coordinates, *Ocean modelling*, *4*(1), 55–88.

Blumberg, A., and G. Mellor (1987), A description of a three-dimensional coastal ocean circulation model., in *Three-dimensional Coastal Ocean Models*, *Coastal and Estuarine Sciences*, vol. 4, edited by N. Heaps., pp. 1–16, American Geophys. Union.

Browning, G., and H.-O. Kreiss (1982), Initializing of the shallow water equations with the open boundaries by the bounded derivative method, *Tellus*, *34*, 334–351.

Browning, G., and H.-O. Kreiss (1986), Scaling and computation of smooth atmospheric motions, *Tellus*, *38*, 295–313.

Budgell, W. P. (2005), Numerical simulation of ice-ocean variability in the Barents Sea region. Towards dynamical downscaling, *Ocean Dynamics*, *55*, 370–387, doi:10.1007/s10236-005-0008-3.

Chapman, D. C. (1985), Numerical treatment of cross-shelf open boundaries in a barotropic coastal ocean model, *J. Phys. Oceanogr.*, *15*, 1060–1075.

Chassignet, E., H. Arango, D. Dietrich, T. Ezer, M. Ghil, D. Haidvogel, C.-C. Ma, A. Mehra, A. Paiva, and Z. Sirkes (2000), DAMÉE-NAB: The base experiments, *Dyn. Atmos. Oceans*, *32*, 155–183.

Chassignet, E., L. Smith, G. Halliwell, and R. Bleck (2003), North Atlantic simulation with the HYbrid Coordinate Ocean Model (HYCOM): Impact of the vertical coordinate choice, reference density, and thermobaricity, *J. Phys. Oceanogr.*, *33*, 2504–2526.

Drange, H., and K. Simonsen (1996), Formulation of air-sea fluxes in the ESOP2 version of MICOM, *Tech. Rep. 125*, NERSC, [Available from Nansen Environmental and Remote Sensing Center, Edv. Griegsvei 3A, N-5037 Bergen, Norway].

Engedahl, H. (1995b), Implementation of the Princeton ocean model (POM/ECOM-3D) at the Norwegian Meteorological Institute (DNMI)., *Research Report 5*, Norwegian Meteorological Institute.

Engedahl, H., and L. P. Røed (1999), Forecasting ocean currents in deep water areas: The Ormen Lange case (1997), *Research Report 80*, Norwegian Meteorological Institute, Box 43 Blindern, N-0313 Oslo, Norway.

Engedahl, H., G. Eriksrød, C. Ulstad, and B. Ådlandsvik (1997), Climatological oceanographic archives covering the Nordic Seas and the Arctic Ocean with adjacent waters, *Research Report 59*, Norwegian Meteorological Institute, Box 43 Blindern, N-0313 Oslo, Norway.

Engedahl, H., A. Lunde, A. Melsom, and X. B. Shi (2001), New schemes for vertical mixing in MI-POM and MICOM, *Research Report 118*, Norwegian Meteorological Institute, ISSN 0332-9879.

Evensen, G., and D. Szabo (2002), NWAG Phase II-A Technical Summary, *Tech. Rep. 215*, Ocean Numerics Ltd, Thormøhlensgt. 47, N–5006 Bergen.

Fairall, C. W., E. F. Bradley, J. E. Hare, A. A. Grachev, and J. B. Edson (2003), Bulk parameterization of air-sea fluxes: Updates and verification for the COARE algorithm, *J. Clim.*, *16*, 571–591.

Flather, R. (1981), Results from a model of the north-east Atlantic relating to the Norwegian coastal current, in *Norwegian Coastal Current Symposium*, vol. II, edited by R. Stre and M. Mork, p. 31, University of Bergen.

Flather, R. A. (1976), A tidal model of the northwest European continental shelf, *Mem. Soc. Roy. Scie. Liege*, *6*(10), 141–164.

Fossum, I. (2006), Analysis of instabilities and mesoscale motion off southern Norway, *J. Geophys. Res.*, *111, C08006*, doi:10.1029/2005JC003228.

Fossum, I., and L. P. Røed (2006), Analysis of instabilities and mesoscale motion in continuously stratified ocean models, *J. Mar. Res.*, *64*, 319–353.

Galperin, B., L. H. Kanta, S. Hassid, and A. Rosati (1988), A quasi-equilibrium energy model for geophysical flows., *J. Atmos. Sc.*, *45*, 55–62.

Gerritsen, H., and A. C. Bijlsma (1988), *Computer Modelling in Ocean Engineering*, chap. Modelling of tidal and wind driven flow: The Dutch Continental Shelf Model, p. 9 pp., Schrefler & Zienckiewicz, Rotterdam, Balkema.

Gjevik, B., E. Nøst, and T. Straume (1990), Atlas of tides on the Shelves of the Norwegian and Barents Seas, *Tech. Rep. F&U-ST 90012 Statoil*, Department of Mathematics, University of Oslo.

Gjevik, B., E. Nøst, and T. Straume (1994), Model simulation of the tides in the Barents Seas, *J. Geophys. Res.*, *99*(C2), 3337–3350.

Griffies, S. M. (2004), *Fundamentals of ocean climate models*, Princeton University Press.

Hackett, B., and H. Engedahl (2000), Numerical model study of slope and Deep Water Currents. PhaseIII: Regional archive evaluation and Ormen Lange hindcast, *Research Report 93*, Norwegian Meteorological Institute, Box 43 Blindern, N-0313 Oslo, Norway.

Hackett, B., and L. P. Røed (1994), Numerical modeling of the Halten Bank area: a validation study, *Tellus*, *46A*, 113–133.

Hackett, B., L. P. Røed, B. Gjevik, E. A. Martinsen, and L. I. Eide (1995), A review of the metocean modeling project (MOMOP). Part 2: Model validation study, in *Quantitative Skill Assessment for Coastal Ocean Models*, *Coastal and Estuarine Studies*, vol. 47, edited by D. R. Lynch and A. M. Davies, pp. 307–327, American Geophysical Union.

Haidvogel, D. B., H. Arango, W. Budgell, B. Cornuelle, E. Curchitser, E. D. Lorenzo, K. Fennel, W. Geyer, A. Hermann, L. Lanerolle, J. Levin, J. McWilliams, A. Miller, A. Moore, T. Powell, A. Shchepetkin, C. Sherwood, R. Signell, J. Warner, and J. Wilkin (2007), Regional ocean forecasting in terrain-following coordinates: Model formulation and skill assessment, *J. Comput. Phys.*, accepted.

Jenkins, A. D., H. Engedahl, B. Hackett, and B. Å. Hjøllo (2001), Validation of water level predictions in Norwegian waters, *Research report no. 105*, Norwegian Meteorological Institute, Oslo, Norway.

Johannessen, J. A., B. Hackett, E. Svendsen, H. Søiland, L. P. Røed, N. G. Winther, J. Albretsen, D. Danielsen, L. Pettersson, M. Skogen, and L. Bertino (2006), Monitoring of the Norwegian coastal zone environment - the MONCOZE approach, in *European Operational Oceanography: Present and Future, Proceedings of the 4th International Conference o n EuroGOOS, 6-9 June 2005, Brest, France*, edited by H. Dahlin, N. C. Flemming, P. Marchand, and S. E. Petersson, pp. 809–815, EuroGOOS Office, SMHI, and European Commission Research Directorate.

Johannessen, J. A., B. Hackett, E. Svendsen, H. Søiland, L. P. Røed, N. Winther, J. Albretsen, D. Danielsen, L. Petterson, M. Skogen, and L. Bertino (2007), Operational oceanography - Challenges and possibilities, in *The Norwegian Coastal Current - Oceanography and Climate*, edited by R. Sætre, pp. 139–150, Tapir Academic Press, Trondheim, Norway.

LaCasce, J. (2005), Statistics of low frequency currents over the western Norwegian shelf and slope I: current meters, *Ocean Dyn.*, *55*, 213–221, doi 10.1007/s10,236–005–0021–6.

LaCasce, J., and H. Engedahl (2005), Statistics of low frequency currents over the western Norwegian shelf and slope II: Model, *Ocean Dyn.*, *55*, 222–237, doi 10.1007/s10,236–005–0022–5.

Large, W. G., J. C. McWilliams, and S. C. Doney (1994), Oceanic vertical mixing: A review and a model with a vertical k-profile boundary layer parameterization., *Rev. Geophys.*, *32*, 363–403.

Laurent, B., K. A. Lisæter, H. Sagen, F. Counillon, N. Winther, M. Stette, L. J. Natvik, G. Evensen, Y. Morel, J. M. B. F., Birol, P. Brasseur, J. Verron, M. Schartau, J. Schroeter, I. A. Burillo, E. Dombrowsky, G. Larnicol, P. Schaeffer, and G. Weller (2004), TOPAZ final report, *Tech. Rep. 251*, Nansen Centre, Bergen, Norway.

Marchesiello, P., J. C. McWilliams, and A. F. Shchepetkin (2001), Open boundary conditions for long-term integration of regional ocean models, *Ocean Mod.*, *3*, 1–20.

Martinsen, E. A., and H. Engedahl (1987), Implementation and testing of a lateral boundary scheme as an open boundary condition in a barotropic ocean model., *Coast. Eng.*, *11*, 603–627.

Martinsen, E. A., H. Engedahl, B. Hackett, H. Tønnesen, O. Høvik, and B. Ådlandsvik (1995), Metocean MOdeling Project: Hindcast simulations of the ocean response to storm events for the Haltenbanken, the Vøringsplateau and the barents sea, *Research report no. 6*, Norwegian Meteorological Institute, Oslo, Norway.

Mauritzen, C. (1996), Production of dense overflow waters feeding the north atlantic across the greenland-scotland ridge. part 1: Evidence for a revised circulation scheme, *Deep Sea Research*, *43*, 769–806.

Mellor, G. L., and T. Yamada (1982), Development of a turbulence closure model for geophysical fluid problems, *Rev. Geophys. Space Phys.*, *20*, 851–875.

Orvik, K. A., and P. Niller (2002), Major pathways of Atlantic water in the northern North Atlantic and Nordic Seas toward Arctic, *Geophys. Res. Lett.*, *29(19)*, 1896, doi:10102.

Orvik, K. A., Ø. Skagseth, and M. Mork (2001), Atlantic inflow to the Nordic seas: current structure and volume fluxes from moored current meters, VM-ADCP and SeaSoar-CTD observations, 1995-1999, *Deep Sea Res., I*, *48*, 937–957.

Poulain, P. M., A. Warn-Varnas, and P. Niller (2001), Near-surface circulation of the Nordic Seas as measured by Lagrangian drifters, *J. Geophys. Res.*, *106*, 2589–2604.

Røed, L. P. (1996), Modeling mesoscale features in the ocean, in *Waves and Nonlinear Processes in Hydrodynamics*, *Fluid Mechanics and its applications*, vol. 34, edited by J. Grue, B. Gjevik, and J. E. Weber, pp. 383–396, Kluwer Academic Publishers.

Røed, L. P. (2006), Conman technical report no. 1: Documentation of models and experimental set-up, *met.no Report 05/2006*, Norwegian Meteorological Institute, Box 43 Blindern, N-0313 Oslo, Norway.

Røed, L. P., and J. Debernard (2004), Description of an integrated flux and sea-ice model suitable for coupling to an ocean and atmosphere model, *met.no Report 4/2004*, Norwegian Meteorological Institute, P.O. Box 43 Blindern, 0313 Oslo, Norway.

Røed, L. P., and I. Fossum (2004), Mean and eddy motion in the Skagerrak/northern North Sea: insight from a numerical model, *Ocean Dynamics*, *54*, 197–220.

Røed, L. P., B. Hackett, B. Gjevik, and L. I. Eide (1995), A review of the metocean modeling project (MOMOP). Part 1: Model comparison study., in *Quantitative Skill Assessment for Coastal Ocean Models*, *Coastal and Estuarine Studies*, vol. 47, edited by D. R. Lynch and A. M. Davies, pp. 285–305, American Geophysical Union.

Shchepetkin, A., and J. McWilliams (2005), The Regional Ocean Modeling System (ROMS): A split-explicit, free-surface, topography-following coordinate ocean model, *Ocean Modelling*, *9*, 347–404.

Shchepetkin, A. F., and J. McWilliams (1998), Quasi-monotone advection schemes based on explicit locally adaptive dissipation, *Mon. Wea. Rev.*, *126*, 1541–1580.

Shchepetkin, A. F., and J. McWilliams (2003), A method for computing horizontal pressure-gradient force in an oceanic model with a non-aligned vertical coordinate, *J. Geophys. Res.*, *108*, 1–34.

Skagseth, Ø., and K. A. Orvik (2002), Identifying fluctuations in the Norwegian Atlantic Slope current by means of empirical orthogonal functions, *Cont. Shelf Res.*, *22*, 547–563.

Smagorinsky, J. (1963), General circulation experiments with the primitive equations, I: The basic experiment, *Mon. wea. Rev.*, *91*, 99–164.

Song, T., and D. Haidvogel (1994), A semi-implicit ocean circulation model using a generalized topography-following coordinate system, *J. Comput. Phys.*, *115*(228-244).

Umlauf, L., and H. Burchard (2003), A generic length-scale equation for geophysical turbulence models, *J. Marine Res.*, *61*, 235–265.

Warner, J. C., C. Sherwood, H. Arango, and R. Signell (2005), Performance of four turbulence closure methods implemented using a generic length scale method, *Ocean Mod.*, *8*, 81–113.

Willebrand, J., B. Barnier, C. Böning, C. Dieterich, P. D. Killworth, C. L. Provost, Y. Jia, J.-M. Molines, and A. L. New (2001), Circulation characteristics in three eddy-permitting models of the north atlantic, *Prog. in Oceanogr.*, *48*, 123–161.

Winther, N. G., Y. Morel, and G. Evensen (2007), Efficiency of high order numerical schemes for momentum advection, *J. Mar. Syst.*, doi:10.1016/j.jmarsys.2006.08.004, in press.